



**HAL**  
open science

## Multimodel estimates of intercontinental source-receptor relationships for ozone pollution

A. Fiore, F. Dentener, O. Wild, C. Cuvelier, M. Schultz, P. Hess, C. Textor,  
M. Schulz, R. Doherty, L. Horowitz, et al.

### ► To cite this version:

A. Fiore, F. Dentener, O. Wild, C. Cuvelier, M. Schultz, et al.. Multimodel estimates of intercontinental source-receptor relationships for ozone pollution. *Journal of Geophysical Research*, 2009, 114 (D4), 10.1029/2008JD010816 . hal-03048083

**HAL Id: hal-03048083**

**<https://hal.science/hal-03048083>**

Submitted on 10 Dec 2020

**HAL** is a multi-disciplinary open access archive for the deposit and dissemination of scientific research documents, whether they are published or not. The documents may come from teaching and research institutions in France or abroad, or from public or private research centers.

L'archive ouverte pluridisciplinaire **HAL**, est destinée au dépôt et à la diffusion de documents scientifiques de niveau recherche, publiés ou non, émanant des établissements d'enseignement et de recherche français ou étrangers, des laboratoires publics ou privés.

## Multimodel estimates of intercontinental source-receptor relationships for ozone pollution

A. M. Fiore,<sup>1</sup> F. J. Dentener,<sup>2</sup> O. Wild,<sup>3</sup> C. Cuvelier,<sup>2</sup> M. G. Schultz,<sup>4</sup> P. Hess,<sup>5</sup> C. Textor,<sup>6,7</sup> M. Schulz,<sup>7</sup> R. M. Doherty,<sup>8</sup> L. W. Horowitz,<sup>1</sup> I. A. MacKenzie,<sup>8</sup> M. G. Sanderson,<sup>9</sup> D. T. Shindell,<sup>10</sup> D. S. Stevenson,<sup>8</sup> S. Szopa,<sup>7</sup> R. Van Dingenen,<sup>2</sup> G. Zeng,<sup>11,12</sup> C. Atherton,<sup>13,14</sup> D. Bergmann,<sup>13</sup> I. Bey,<sup>15</sup> G. Carmichael,<sup>16</sup> W. J. Collins,<sup>9</sup> B. N. Duncan,<sup>17</sup> G. Faluvegi,<sup>10</sup> G. Folberth,<sup>15,18</sup> M. Gauss,<sup>19</sup> S. Gong,<sup>20</sup> D. Hauglustaine,<sup>7,21</sup> T. Holloway,<sup>22</sup> I. S. A. Isaksen,<sup>19</sup> D. J. Jacob,<sup>23</sup> J. E. Jonson,<sup>24</sup> J. W. Kaminski,<sup>25</sup> T. J. Keating,<sup>26</sup> A. Lupu,<sup>25</sup> E. Marmer,<sup>2</sup> V. Montanaro,<sup>27</sup> R. J. Park,<sup>23,28</sup> G. Pitari,<sup>27</sup> K. J. Pringle,<sup>9,29</sup> J. A. Pyle,<sup>11</sup> S. Schroeder,<sup>4</sup> M. G. Vivanco,<sup>30</sup> P. Wind,<sup>24</sup> G. Wojcik,<sup>31</sup> S. Wu,<sup>23,32</sup> and A. Zuber<sup>33</sup>

Received 21 July 2008; revised 5 November 2008; accepted 26 November 2008; published 17 February 2009.

[1] Understanding the surface O<sub>3</sub> response over a “receptor” region to emission changes over a foreign “source” region is key to evaluating the potential gains from an international approach to abate ozone (O<sub>3</sub>) pollution. We apply an ensemble of 21 global and hemispheric chemical transport models to estimate the spatial average surface O<sub>3</sub> response over east Asia (EA), Europe (EU), North America (NA), and south Asia (SA) to 20% decreases in anthropogenic emissions of the O<sub>3</sub> precursors, NO<sub>x</sub>, NMVOC, and CO (individually and combined), from each of these regions. We find that the ensemble mean surface O<sub>3</sub> concentrations in the base case (year 2001) simulation matches available observations throughout the year over EU but overestimates them by >10 ppb during summer and early fall over the eastern United States and Japan. The sum of the O<sub>3</sub> responses to NO<sub>x</sub>, CO, and NMVOC decreases separately is approximately equal to that from a simultaneous reduction of all precursors. We define a continental-scale “import sensitivity” as the ratio of the O<sub>3</sub> response to the 20% reductions in foreign versus

<sup>1</sup>NOAA Geophysical Fluid Dynamics Laboratory, Princeton, New Jersey, USA.

<sup>2</sup>Institute for Environment and Sustainability, DG-Joint Research Centre, European Commission, Ispra, Italy.

<sup>3</sup>Department of Environmental Science, Lancaster University, Lancaster, UK.

<sup>4</sup>ICG-II, Forschungszentrum Jülich, Jülich, Germany.

<sup>5</sup>Biological and Environmental Engineering, Cornell University, Ithaca, New York, USA.

<sup>6</sup>GMES France Atmosphère, Service d'Aéronomie, INSU, Université Pierre et Marie Curie, CNRS, Paris, France.

<sup>7</sup>Laboratoire des Sciences du Climat et de l'Environnement, CEA, IPSL, UVSQ, CNRS, Gif-sur-Yvette, France.

<sup>8</sup>School of GeoSciences, University of Edinburgh, Edinburgh, UK.

<sup>9</sup>Met Office Hadley Centre, Exeter, UK.

<sup>10</sup>NASA Goddard Institute for Space Studies, Columbia University, New York, New York, USA.

<sup>11</sup>National Centre for Atmospheric Science, Department of Chemistry, University of Cambridge, Cambridge, UK.

<sup>12</sup>Now at National Institute of Water and Atmospheric Research Ltd., Omakau, New Zealand.

<sup>13</sup>Atmospheric Earth and Energy Division, Lawrence Livermore National Laboratory, Livermore, California, USA.

<sup>14</sup>Now at Gordon and Betty Moore Foundation, San Francisco, California, USA.

<sup>15</sup>Laboratoire de Modélisation de la Chimie Atmosphérique, EPFL, Lausanne, Switzerland.

<sup>16</sup>Center for Global and Regional Environmental Research, College of Engineering, University of Iowa, Iowa City, Iowa, USA.

<sup>17</sup>Goddard Earth Sciences and Technology Center, UMBC, Baltimore, Maryland, USA.

<sup>18</sup>Now at Met Office Hadley Centre, Exeter, UK.

<sup>19</sup>Department of Geosciences, University of Oslo, Oslo, Norway.

<sup>20</sup>Air Quality Research Division, Science and Technology Branch, Environment Canada, Toronto, Ontario, Canada.

<sup>21</sup>Life, Earth and Environmental Sciences, European Science Foundation, Strasbourg, France.

<sup>22</sup>Center for Sustainability and the Global Environment, Nelson Institute for Environmental Studies, University of Wisconsin-Madison, Madison, Wisconsin, USA.

<sup>23</sup>Atmospheric Chemistry Modeling Group, Harvard University, Cambridge, Massachusetts, USA.

<sup>24</sup>Norwegian Meteorological Institute, Oslo, Norway.

<sup>25</sup>Center for Research in Earth and Space Science, York University, Toronto, Ontario, Canada.

<sup>26</sup>Office of Air and Radiation, Environmental Protection Agency, Washington, D. C., USA.

<sup>27</sup>Physics Department, University of L'Aquila, L'Aquila, Italy.

<sup>28</sup>Now at School of Earth and Environmental Sciences, Seoul National University, Seoul, South Korea.

<sup>29</sup>Now at Max Planck Institute for Chemistry, Mainz, Germany.

<sup>30</sup>Atmospheric Pollution Unit, CIEMAT, Madrid, Spain.

<sup>31</sup>Atmospheric Effects Group, Information Technology Sector, Northrop Grumman Corporation, Chantilly, Virginia, USA.

<sup>32</sup>Now at Department of Geological and Mining Engineering and Sciences and Department of Civil and Environmental Engineering, Michigan Technological University, Houghton, Michigan, USA.

<sup>33</sup>Environment Directorate General, European Commission, Brussels, Belgium.

“domestic” (i.e., over the source region itself) emissions. For example, the combined reduction of emissions from the three foreign regions produces an ensemble spatial mean decrease of 0.6 ppb over EU (0.4 ppb from NA), less than the 0.8 ppb from the reduction of EU emissions, leading to an import sensitivity ratio of 0.7. The ensemble mean surface O<sub>3</sub> response to foreign emissions is largest in spring and late fall (0.7–0.9 ppb decrease in all regions from the combined precursor reductions in the three foreign regions), with import sensitivities ranging from 0.5 to 1.1 (responses to domestic emission reductions are 0.8–1.6 ppb). High O<sub>3</sub> values are much more sensitive to domestic emissions than to foreign emissions, as indicated by lower import sensitivities of 0.2 to 0.3 during July in EA, EU, and NA when O<sub>3</sub> levels are typically highest and by the weaker relative response of annual incidences of daily maximum 8-h average O<sub>3</sub> above 60 ppb to emission reductions in a foreign region (<10–20% of that to domestic) as compared to the annual mean response (up to 50% of that to domestic). Applying the ensemble annual mean results to changes in anthropogenic emissions from 1996 to 2002, we estimate a Northern Hemispheric increase in background surface O<sub>3</sub> of about 0.1 ppb a<sup>-1</sup>, at the low end of the 0.1–0.5 ppb a<sup>-1</sup> derived from observations. From an additional simulation in which global atmospheric methane was reduced, we infer that 20% reductions in anthropogenic methane emissions from a foreign source region would yield an O<sub>3</sub> response in a receptor region that roughly equals that produced by combined 20% reductions of anthropogenic NO<sub>x</sub>, NMVOC, and CO emissions from the foreign source region.

**Citation:** Fiore, A. M., et al. (2009), Multimodel estimates of intercontinental source-receptor relationships for ozone pollution, *J. Geophys. Res.*, 114, D04301, doi:10.1029/2008JD010816.

## 1. Introduction

[2] Reducing aerosol and ozone (O<sub>3</sub>) levels in surface air would improve public health as exposure to these atmospheric constituents aggravates respiratory illness and may lead to premature mortality [World Health Organization, 2005]. Findings from numerous observational and modeling studies indicate that long-range transport of pollutants degrade air quality over remote continents [e.g., Wilkening et al., 2000; Holloway et al., 2003; Akimoto, 2003]. Satellite images of aerosols, particularly dust and smoke, illustrate the capacity for dust storms and biomass burning to influence tropospheric composition on a hemispheric scale [e.g., Husar et al., 2001]. Ground-based measurements of aerosol composition provide evidence for a foreign influence in surface air; for example, the presence of smoke from Siberian fires and dust from Asia and Africa over the United States [e.g., Prospero, 1999; Jaffe et al., 2003a, 2004]. In contrast, attributing O<sub>3</sub> pollution to a specific source region is complicated by the interplay of processes influencing intercontinental transport (export from the source region; evolution in transit due to chemical production, chemical and depositional losses, and dilution; and mixing with surface air over the receptor region), and by a large hemispheric background and the dominance of local emissions in contributing to high-O<sub>3</sub> events [e.g., Derwent et al., 2003; Fiore et al., 2003; Goldstein et al., 2004; Jonson et al., 2005]. Given the difficulty of diagnosing O<sub>3</sub> source-receptor (SR) relationships (i.e., the change in O<sub>3</sub> over a receptor region produced by emission changes within a source region) from observations, estimates of these relationships rely heavily on models. Here, we use an ensemble of 21 global and hemispheric chemical transport models (CTMs) to quantify the impact of O<sub>3</sub> precursor emissions from four major continental-scale source regions in the Northern Hemisphere on surface O<sub>3</sub> in

the same four “receptor” regions (Figure 1).<sup>1</sup> Prior studies indicate that multimodel mean results better represent a range of observations than any individual model [Schulz et al., 2006; Stevenson et al., 2006; Reichler and Kim, 2008]; the range of results across individual models provides a measure of uncertainty in our understanding as represented in the current generation of CTMs.

[3] Tropospheric O<sub>3</sub> is produced via the photochemical oxidation of volatile organic compounds (VOC) and carbon monoxide (CO) in the presence of nitrogen oxides (NO<sub>x</sub>). To date, regulations to abate surface O<sub>3</sub> pollution address emissions of the traditional O<sub>3</sub> precursors (NO<sub>x</sub>, nonmethane VOC (NMVOC) and CO) which react within hours-to-weeks to produce a “short-term” O<sub>3</sub> response. By altering hydroxyl radical (OH) concentrations, perturbations to emissions of these species affect the lifetime of methane (CH<sub>4</sub>), the most abundant atmospheric VOC and a major precursor to O<sub>3</sub> in the remote troposphere [Crutzen, 1973; Prather, 1996; Daniel and Solomon, 1998; Fuglestedt et al., 1999; Derwent et al., 2001; Collins et al., 2002], producing a “long-term” influence on surface O<sub>3</sub>. This “long-term” O<sub>3</sub> response occurs on the methane perturbation timescale, is spatially distributed following the O<sub>3</sub> production from CH<sub>4</sub>, and somewhat offsets the O<sub>3</sub> response to perturbations in surface NO<sub>x</sub> emissions, while enhancing the response to NMVOC and CO emission changes. [Wild et al., 2001; West et al., 2007]. Anthropogenic CH<sub>4</sub> emissions have also been shown to contribute directly to O<sub>3</sub> in surface air [Fiore et al., 2002a; Dentener et al., 2005; West et al., 2007; Fiore et al., 2008]. The contributions to surface O<sub>3</sub> over a receptor region both from CH<sub>4</sub> and from the foreign emissions of the traditional O<sub>3</sub> precursors

<sup>1</sup>Auxiliary material data sets are available at <ftp://ftp.agu.org/apend/jd/2008JD010816>.

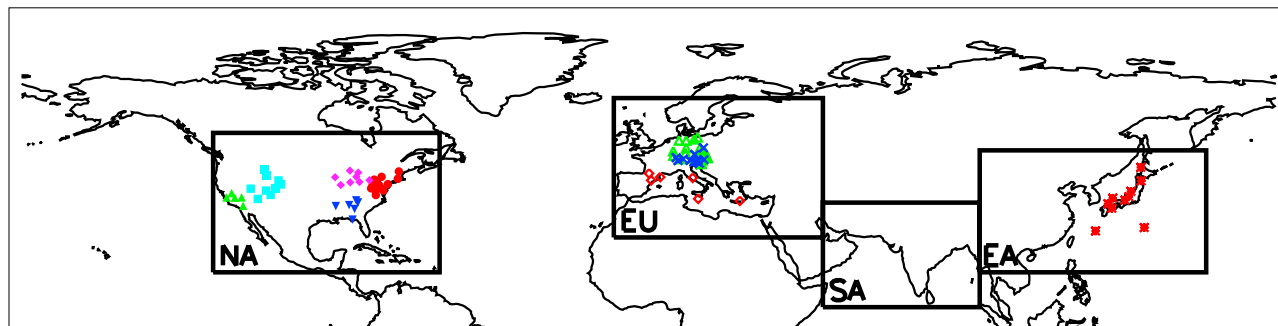


**Figure 1.** The HTAP source-receptor regions: NA ( $15^{\circ}\text{N}$ – $55^{\circ}\text{N}$ ;  $60^{\circ}\text{W}$ – $125^{\circ}\text{W}$ ), EU ( $25^{\circ}\text{N}$ – $65^{\circ}\text{N}$ ;  $10^{\circ}\text{W}$ – $50^{\circ}\text{E}$ ), EA ( $15^{\circ}\text{N}$ – $50^{\circ}\text{N}$ ;  $95^{\circ}\text{E}$ – $160^{\circ}\text{E}$ ), and SA ( $5^{\circ}\text{N}$ – $35^{\circ}\text{N}$ ;  $50^{\circ}\text{E}$ – $95^{\circ}\text{E}$ ). Sites marked with the same symbols are used to produce the subregional averages in Figure 2, from the European Monitoring and Evaluation Programme (EMEP) in the Mediterranean (red diamonds; Figure 2a) and central Europe (green open triangles for sites below 1 km and blue crosses for sites >1 km; Figures 2b and 2c, respectively); from the U.S. Clean Air Status and Trends Network (CASTNet) in the northeast (red circles; Figure 2d) southwest (green triangles; Figure 2e), southeast (dark blue inverted triangles; Figure 2f), Great Lakes (pink diamonds; Figure 2g), and mountainous west (cyan squares; Figure 2h), and from the Acid Deposition Monitoring Network in East Asia (EANET) in Japan (red asterisks; Figure 2i).

are generally considered to be part of the “background”  $\text{O}_3$  level (along with natural precursor emissions), and have not generally been considered in air pollution mitigation strategies.

[4] Analysis of observations at northern midlatitudes indicate that background  $\text{O}_3$  has been increasing in recent years, although estimates vary, with some revealing little change [e.g., Vingarzan, 2004; Task Force on Hemispheric Transport of Air Pollution (TF HTAP), 2007; Oltmans et al., 2006; Derwent et al., 2007; Schultz et al., 2007]. Several modeling studies suggest that projected increases in emissions around the globe will enhance hemispheric background  $\text{O}_3$  in the coming decades, potentially offsetting efforts to improve regional air quality via controls on domestic precursor emissions [e.g., Jacob et al., 1999; Yienger et al., 2000; Collins et al., 2000; Fiore et al., 2002a; Dentener et al., 2005; Derwent et al., 2006; Szopa et al., 2006; Ellingsen et al., 2008]. Efforts to improve air quality typically focus on controlling local and regional sources. In nations where  $\text{O}_3$  precursors have been regulated for decades, the combination of increasing hemispheric background levels and mounting control costs could make pursuing international cooperation an attractive option [Keating et al., 2004; Bergin et al., 2005; Solberg et al., 2005]. An international approach to air quality management will require a strong scientific understanding of the SR relationships between continents and nations.

[5] Under the United Nations Economic Commission for Europe (UNECE) Convention on Long Range Transboundary Air Pollution (CLRTAP), the Task Force on Hemispheric Transport of Air Pollution (TF HTAP; www.htap.org) was established to advance the understanding of hemispheric transport of air pollutants in the Northern Hemisphere. A major TF HTAP activity is to coordinate a multimodel effort to quantify and estimate uncertainties in intercontinental SR relationships for  $\text{O}_3$ , aerosols, mercury, and persistent organic pollutants. Companion manuscripts investigate  $\text{NO}_y$  deposition [Sanderson et al., 2008], transport with idealized tracers (M. Schultz et al., manuscript in preparation, 2009), the Arctic as a receptor region [Shindell et al., 2008], and aerosols (Schulz et al., manuscript in preparation, 2009).

[6] Prior estimates for intercontinental SR relationships differ by factors of about 2 to 6 for a given SR pair among source regions at northern midlatitudes [TF HTAP, 2007, and references therein]. Comparison among prior studies, however, is limited by methodological differences, including definitions of source and receptor regions, reported metrics, period of analysis, and SR calculation method [TF HTAP, 2007]. Observational analyses have compared concentration differences in air masses originating from a source region versus a background value [e.g., Huntrieser et al., 2005; Derwent et al., 1998; Jaffe et al., 2003b]. A suite of methods for source attribution have been applied in models, including marking tracers by region of  $\text{O}_3$  production [e.g., Jaeglé et al., 2003; Derwent et al., 2004], labeling by the regional  $\text{NO}_x$  source contributing to  $\text{O}_3$  production [Hess and Lamarque, 2007], and perturbing regional emissions [e.g., Jacob et al., 1999; Yienger et al., 2000; Wild and Akimoto, 2001; Fiore et al., 2002b; Auvray and Bey, 2005].

[7] The approach adopted here builds upon these previous studies by applying a consistent experimental design across multiple models to provide an estimate of SR relationships throughout the year. Specifically, we investigate the changes in surface  $\text{O}_3$  resulting from fixed percentage reductions in anthropogenic  $\text{O}_3$  precursors ( $\text{NO}_x$ , CO,  $\text{CH}_4$ , and NMVOC). We first describe the modeling framework (section 2) and evaluate the base case simulations with observations of surface  $\text{O}_3$  (section 3). Our analysis focuses on two continental-scale SR metrics: (1) the response, defined as the spatially averaged absolute change in  $\text{O}_3$  concentrations over a receptor region due to emission changes in a source region, and (2) the “import sensitivity,” defined as the ratio of the sum of the spatially averaged changes in surface  $\text{O}_3$  in a continental receptor region resulting from perturbations to precursor emissions in the three foreign source regions to the surface  $\text{O}_3$  change resulting from the same percentage perturbation to domestic emissions (i.e., emissions within the continental receptor region; section 4). We then examine the response of surface  $\text{O}_3$  to changes in  $\text{CH}_4$  levels (section 5). In an effort to relate our results more directly to statistics commonly employed in air quality management,

**Table 1.** Model Ensemble Annual Mean (Median)  $\pm 1$  Standard Deviation in Total and Anthropogenic Emissions of  $\text{NO}_x$ , NMVOC, and CO, Globally and for the Regions in Figure 1<sup>a</sup>

Total Emissions	Global	NA	EU	EA	SA
$\text{NO}_x$	46.5(46.2) $\pm$ 5.7	8.5(8.7) $\pm$ 0.8	8.4(8.4) $\pm$ 1.1	7.1(6.9) $\pm$ 1.4	3.3(3.3) $\pm$ 0.5
NMVOC	630(623) $\pm$ 221	62(57) $\pm$ 24	37(34) $\pm$ 13	48(47) $\pm$ 14	33(34) $\pm$ 8.8
CO	1060(1090) $\pm$ 135	130(130) $\pm$ 20	90(81) $\pm$ 25	150(150) $\pm$ 29	97(96) $\pm$ 23
Anthropogenic Emissions					
$\text{NO}_x$	32.5(29.4) $\pm$ 6.0	7.4(7.3) $\pm$ 0.4	7.3(7.5) $\pm$ 0.6	6.0(5.5) $\pm$ 1.4	2.4(2.2) $\pm$ 0.4
NMVOC	96.8(92.3) $\pm$ 41.8	16(16) $\pm$ 7.0	19(20) $\pm$ 11	16(17) $\pm$ 6.5	10(10) $\pm$ 3.9
CO	661(563) $\pm$ 214	101(103) $\pm$ 19	80(70) $\pm$ 23	133(123) $\pm$ 35	80(79) $\pm$ 18

<sup>a</sup>Units:  $\text{NO}_x$ , Tg N a<sup>-1</sup>; NMVOC, Tg C a<sup>-1</sup>; and CO, Tg a<sup>-1</sup>. Emissions in individual models are provided in auxiliary material Data Sets S2 and S3.

we also analyze the response of a threshold indicator of air quality to emission changes (section 6). Finally, we apply our SR relationships to evaluate the role of reported trends in Asian emissions on trends in northern midlatitude surface  $\text{O}_3$  observed in recent decades (section 7).

## 2. Model Simulations and Emissions

[8] Simulations designed to estimate intercontinental source-receptor (SR) relationships for  $\text{O}_3$  were conducted in 21 chemical transport models (CTMs) (auxiliary material Data Set S1). Initial results were reported by *TFHTAP* [2007]; we expand here upon that analysis. Most models were driven by meteorological fields from one of several reanalysis centers (either prescribed directly or via linear relaxation) for the year 2001, although four models were general circulation models with meteorology generated on the basis of observed sea surface temperatures for 2001 (auxiliary material Data Set S1). Model horizontal resolution ranged from  $5^\circ \times 5^\circ$  to  $1^\circ \times 1^\circ$ , with resolutions of  $3^\circ \times 3^\circ$  or finer in about half of the models, similar to the ACCENT/AR4 intercomparison [Dentener et al., 2006; Stevenson et al., 2006].  $\text{CH}_4$  concentrations were set to a uniform mixing ratio of 1760 ppb and modeling groups were requested to use their best estimate of  $\text{O}_3$  precursor emissions for the year 2001 (auxiliary material Data Set S2); the use of different emission inventories contributes to the intermodel differences in our results.

[9] We consider four major source regions at northern mid-latitudes (Figure 1): east Asia (EA), Europe and northern Africa (EU), North America (NA), and south Asia (SA). The EU and EA regions span roughly equivalent areas ( $2.1 \times 10^7$  and  $2.3 \times 10^7$  km<sup>2</sup>), with NA somewhat larger ( $2.6 \times 10^7$  km<sup>2</sup>) and nearly twice the area of SA ( $1.5 \times 10^7$  km<sup>2</sup>). Anthropogenic emissions of  $\text{NO}_x$  and NMVOC from EU, NA, and EA are similar in the model ensemble mean ( $\mu$ ) to within  $\sim 30\%$  (Table 1; auxiliary material Data Set S3). The standard deviation ( $\sigma$ ) indicates the diversity of the emission inventories used in the models, with the smallest relative intermodel spread for anthropogenic  $\text{NO}_x$  emissions in EU and NA ( $\sigma/\mu < 10\%$ ) and the largest spread for anthropogenic NMVOC from EU ( $\sigma/\mu = 58\%$ ). A comparison of the model ensemble mean anthropogenic and total (which also includes biomass burning and biogenic contributions) emissions in Table 1 shows a dominant contribution ( $>70\%$ ) from anthropogenic  $\text{NO}_x$  and CO in all regions considered. For the ensemble mean NMVOC emissions, biogenic emissions dominate in all regions except for EU where anthropogenic and biogenic contributions are approximately equal.

[10] Relative to SR1, we conduct 16 sensitivity simulations in which anthropogenic emissions of the traditional  $\text{O}_3$  precursors ( $\text{NO}_x$ , NMVOC, and CO) are reduced by 20% individually (simulations SR3, SR4, and SR5, respectively) and jointly along with aerosols (“ALL”; simulation SR6) within each of the four source regions in Figure 1. These simulations are labeled hereafter according to the respective emission scenario and the region in which emission reductions were applied (e.g., SR3EA identifies the simulations with 20% reductions of anthropogenic  $\text{NO}_x$  emissions within east Asia). An additional sensitivity simulation was conducted in which the  $\text{CH}_4$  mixing ratio was decreased by 20% (to 1408 ppb) and other  $\text{O}_3$  precursor emissions were not changed (SR2). The results from this simulation are interpreted in section 5.3 in an effort to compare more directly the probable ozone response from regional reductions of anthropogenic  $\text{CH}_4$  emissions to that from the regional reductions in emissions of other  $\text{O}_3$  precursors simulated in the SR3, SR4, SR5 and SR6 experiments. All simulations were conducted for a full year, following a minimum of six months initialization, a sufficient time for the simulated trace gas concentrations to fully respond to the imposed emission or concentration perturbations given our use of uniform  $\text{CH}_4$  mixing ratios; responses on longer timescales are diagnosed in section 5.2. The number of models participating in each of the sensitivity simulations ranges from 13 to 18 (auxiliary material Data Set S4).

[11] The perturbation magnitude of 20% reflects a compromise between producing a clear signal in the  $\text{O}_3$  simulations and applying a sufficiently small perturbation to allow the results to be scaled linearly to different size perturbations. Under the ACCENT/AR4 Experiment 2, Stevenson et al. [2006] found a broadly linear relationship between the 26-model mean tropospheric  $\text{O}_3$  burden and global  $\text{NO}_x$  emissions within the  $\pm 50\%$  range of present-day emissions considered in that study, although those simulations did not exclusively change  $\text{NO}_x$  emissions. The scalability of our results to perturbations of other magnitudes is examined further for  $\text{NO}_x$  in section 4.2, and has been shown to hold for the  $\text{O}_3$  response to changes in  $\text{CH}_4$  over the range of present-day anthropogenic emissions [Fiore et al., 2008]. We approximate the  $\text{O}_3$  response to simultaneous reductions in multiple regions as the sum of the  $\text{O}_3$  responses to the individual regional reductions. Companion work suggests that such linearity should hold for the NMVOC and CO emission reductions but that this approach may underestimate the  $\text{O}_3$  response to  $\text{NO}_x$  emission reductions imposed simultaneously in multiple regions (S. Wu et al.,

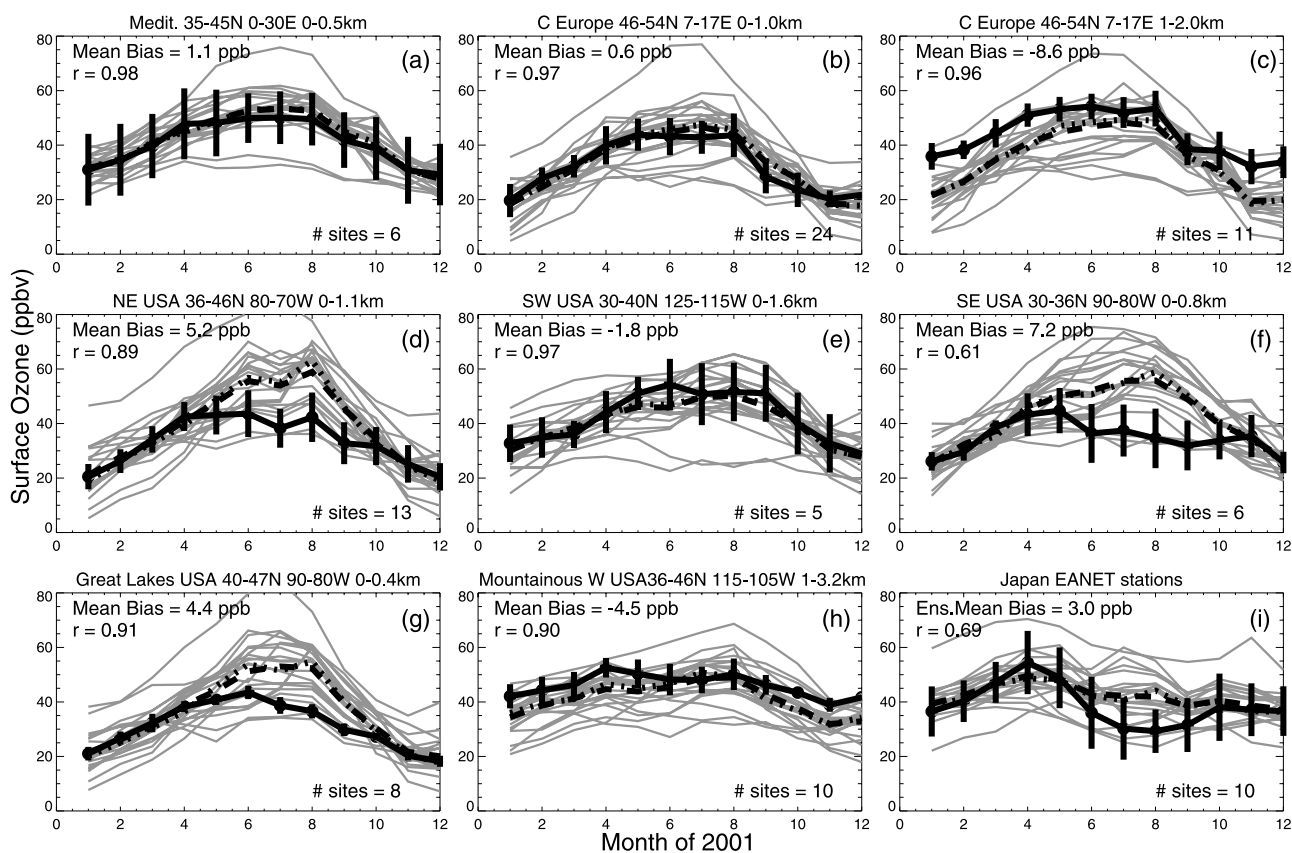


**Figure 2.** Monthly mean surface  $O_3$  concentrations (ppbv) for the year 2001. Observed values (black circles) represent the average of all sites falling within the given latitude, longitude, and altitude boundaries and denoted by the symbols in Figure 1; vertical black lines depict the standard deviation across the sites. Monthly mean  $O_3$  in the surface layer of the SR1 simulations from the 21 models are first sampled at the model grid cells containing the observational sites and then averaged within subregions (gray lines); these spatial averages from each model are used to determine the multimodel ensemble median (black dotted line) and mean (black dashed line). Observations are from CASTNET (<http://www.epa.gov/castnet/>) in the United States, from EMEP (<http://www.nilu.no/projects/ccc/emepdata.html>) in Europe, and from EANET (<http://www.eanet.cc/eanet.html>) in Japan.

Chemical nonlinearities in relating intercontinental ozone pollution to anthropogenic emissions, submitted to *Geophysical Research Letters*, 2009; see also section 4.2).

### 3. Model Evaluation With Surface Observations

[12] We first calculate the spatial average (area-weighted) surface  $O_3$  mixing ratios over each of the four regions in Figure 1, using the values from the lowest-level grid boxes in each model. In the base simulation (SR1), the 21-model annual spatial mean surface  $O_3$  mixing ratios and their standard deviations (across models) over the four continental source regions in Figure 1 are similar:  $36.2 \pm 3.9$  ppb for NA,  $37.8 \pm 4.5$  for EU,  $35.8 \pm 3.0$  for EA, and  $39.6 \pm 4.0$  for SA. The largest ensemble mean peak-to-peak amplitude (difference between the maximum and minimum months) occurs in EU ( $19.8 \pm 5.9$  ppb), possibly reflecting  $NO_x$  titration in the stronger wintertime boundary layer compared to the other regions ( $10.4 \pm 2.6$  for NA;  $12.7 \pm 3.2$  for EA, and  $14.8 \pm 6.0$  for SA).

[13] A major challenge to assessing model skill at representing the  $O_3$  response to foreign (or domestic) emission

changes arises from the difficulty of directly observing these relationships (particularly in surface air). Testing the models with simultaneous measurements of  $O_3$  and related species is preferable [e.g., Sillman, 1999]; such observations are mainly limited to intensive field campaigns, which are the focus of an ongoing TF HTAP multimodel study. A companion study will evaluate the models with the ozonesonde network (J. E. Jonson et al., manuscript in preparation, 2009). Many of the models in our study have been compared with ozone observations for the year 2000 as part of the ACCENT/AR4 Experiment 2 study [e.g., Dentener et al., 2006; Stevenson et al., 2006; Ellingsen et al., 2008]. Annual mean surface  $O_3$  concentrations were within 5 ppb of the measurements in the United States, China, and central Europe (out of total observed values of 40–50 ppb) [Dentener et al., 2006]. Overestimates of 10–15 ppb (out of total observed values of 20–40 ppb) were found in Africa, India, and the Mediterranean, for reasons not yet understood [Dentener et al., 2006; Ellingsen et al., 2008].

[14] Owing to limited availability of surface  $O_3$  measurements over India, China, and Africa, we focus here on the widespread observational networks in the United States, Europe, and Japan (Figure 2). While spatially averaged con-

concentrations over the regions in Figure 2 often differ by more than 15 ppb in the individual models, the model ensemble mean generally captures the observed seasonal cycle and is close to the observed regional mean. A wide range of simulated tropospheric O<sub>3</sub> budgets has been documented in the literature, attributed in part to factors that are likely to contribute to intermodel variability in simulated surface O<sub>3</sub> concentrations, such as differences in surface emissions of NO<sub>x</sub> and isoprene, as well as in model treatment of dry deposition, heterogeneous chemistry and the organic nitrates from isoprene [Stevenson *et al.*, 2006; Wu *et al.*, 2007; Wild, 2007; Ellingsen *et al.*, 2008].

[15] We separate the observational sites at low elevations from those at higher altitudes in Figure 2 since high-altitude sites more frequently sample free tropospheric air and thus are better suited to detecting hemispheric pollutant transport (which occurs most efficiently in the free troposphere) prior to mixing with local pollutant signals in the planetary boundary layer [Cooper and Moody, 2000; Trickl *et al.*, 2003; Weiss-Penzias *et al.*, 2006]. All models are sampled at the lowest level (surface) within the grid cell corresponding to each site location (including for high-altitude sites). At the high-altitude sites (Figures 2c and 2h), the models tend to underestimate O<sub>3</sub> concentrations. Steep topographic gradients that are averaged out within one model grid cell, particularly over Europe, may be responsible if the measurements are more representative of the free troposphere than the models' surface layer (where O<sub>3</sub> deposition leads to lower concentrations); additionally, the coarse resolution of global models cannot represent local orographically driven flows or sharp gradients in mixing depths.

[16] The model ensemble mean and median exhibit little bias at low-altitude European sites and capture the seasonal cycle (Figures 2a and 2b), an apparent improvement over the underestimate in summer months found by Ellingsen *et al.* [2008]. In contrast, the multimodel mean overestimates the observed summertime surface O<sub>3</sub> concentrations over Japan (bias of 12 ppb; Figure 2i) and in the eastern U.S. (bias greater than 14 ppb in July in Figures 2d, 2f, and 2g). The observed summer minimum in O<sub>3</sub> over Japan occurs during the wet season of the Asian monsoon. Results from the MICS-Asia regional model intercomparison suggest that the positive model bias in this season may stem from inadequate representation of southwesterly inflow of clean marine air [Han *et al.*, 2008; Holloway *et al.*, 2008]. Examination of intermodel differences in this region with the TF HTAP idealized tracer transport simulations (Schultz *et al.*, manuscript in preparation, 2009) should provide further insights into the source of this problem.

[17] Ellingsen *et al.* [2008] also found an overestimate of surface O<sub>3</sub> levels in July through September for the year 2000 over the Great Lakes and in June through September over the southeastern United States. In July and August, however, the ensemble median value fell within the standard deviation of the observations. We find that the observed July and August average O<sub>3</sub> decreased by 10 ppb from 2000 to 2001; the larger model error shown in Figure 2 than found by Ellingsen *et al.* [2008] suggests that the model ensemble mean does not capture the observed interannual variability over the eastern United States, although our use of different emission inventories than those used by Ellingsen *et al.* [2008] may also play a role. The bias is particularly large

over the southeastern United States where uncertainties in isoprene-NO<sub>x</sub>-O<sub>3</sub> chemistry may contribute; smaller biogenic NMVOC emissions over Europe (difference between total and anthropogenic NMVOC in Table 1) would lessen the impact of any problems in this chemistry on surface O<sub>3</sub> concentrations there. The bias is not driven by nighttime processes since restricting our comparison to afternoon hours does not yield any improvement (auxiliary material Figure S1). The sensitivity of surface O<sub>3</sub> over all regions to the three foreign source regions is strongest in spring and late autumn (section 4.1) when the model ensemble mean matches the observed values in all regions. We further examine the potential influence of the bias on the predicted source-receptor relationships during summer in section 4.3.

## 4. Source-Receptor Relationships for NO<sub>x</sub>, NMVOC, and CO

### 4.1. Model Ensemble Mean Results

[18] Figure 3 (and auxiliary material Data Set S4) shows the annual average surface O<sub>3</sub> response in the receptor regions to 20% regional reductions of anthropogenic NO<sub>x</sub>, CO, NMVOC emissions, individually and all together ("ALL"), as well as the sum of the responses to emission perturbations in the three foreign source regions (for a discussion of linearity see section 4.2). In most receptor regions, O<sub>3</sub> responds strongly to NO<sub>x</sub>, followed by NMVOC and CO, respectively. An exception occurs for EU emissions where the model ensemble O<sub>3</sub> response to NMVOC is comparable to that from NO<sub>x</sub>. The relative dominance of NO<sub>x</sub> diminishes when the long-term feedback through CH<sub>4</sub> is taken into account (section 5.2). For all SR pairs, domestic emission reductions are most effective at reducing surface O<sub>3</sub>. Surface O<sub>3</sub> also decreases when emissions are reduced in a foreign source region, sometimes by >10% of the decrease attained from the same percentage reduction of domestic emissions (Figure 3 and asterisked entries in auxiliary material Data Set S4). In some cases, annual mean responses to foreign emissions are as large as ~50% of the response to domestic emissions, as occurs for NA NO<sub>x</sub>, CO, and ALL on surface O<sub>3</sub> in EU; for EU NMVOC on surface O<sub>3</sub> in SA; and for EA CO on surface O<sub>3</sub> in NA and EU.

[19] We next examine seasonality in these SR relationships, beginning with the seasonal cycle in the O<sub>3</sub> response to domestic emission reductions (solid circles in Figure 4). Over all regions, the domestic response to the 20% decrease in CO emissions (~0.1 ppb) varies little during the year while the response to NO<sub>x</sub> exhibits the strongest seasonality (maximum of >1 ppb). Over EU, NO<sub>x</sub> reductions increase the model ensemble mean O<sub>3</sub> from November to March. The surface O<sub>3</sub> decrease from NMVOC emission reductions is largest in boreal winter (up to ~0.5 ppb over EU, though seasonality is weak), when biogenic emissions, radiation, and humidity are at their seasonal minimum and O<sub>3</sub> production is more sensitive to anthropogenic NMVOC [Jacob *et al.*, 1995]. The seasonality of the domestic response to ALL is largely driven by NO<sub>x</sub>, peaking in summer for NA, EU, and EA, and in October through March for SA. The different seasonality over SA reflects the influence of the Asian monsoon (wet season during boreal summer).

[20] We find that intercontinental transport contributes most to surface O<sub>3</sub> concentrations at northern midlatitudes

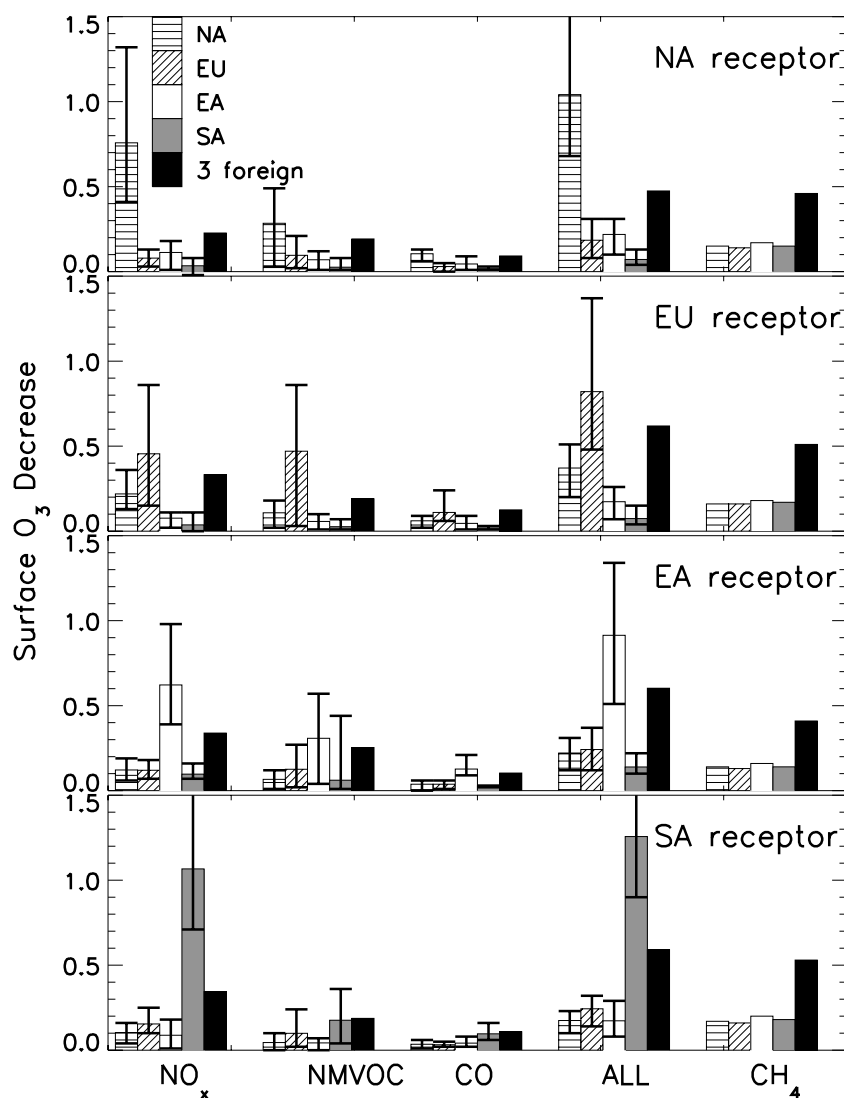


**Figure 3.** Model ensemble surface O<sub>3</sub> decrease (ppb), annually and spatially averaged over the receptor regions (Figure 1) from 20% reductions of anthropogenic O<sub>3</sub> precursor emissions individually (NO<sub>x</sub>, NMVOC, and CO), combined (ALL), and CH<sub>4</sub> within the source regions (see also auxiliary material Data Set S4). Each group of bars includes results from the four regional perturbation experiments: NA (horizontal lines), EU (angled lines), EA (white), and SA (gray), as well as the sum of the impacts from the three foreign source regions (black). The responses to the global CH<sub>4</sub> level reduction are estimated as described in section 5.3 using the model ensemble mean results from SR1–SR2 (auxiliary material Data Set S4). The whiskers span the full range of the individual model responses.

during boreal spring and fall (solid circles in Figure 5), reflecting a combination of more frequent storm tracks that enhance ventilation of the continental boundary layer, more efficient transport in stronger midlatitude westerly flow in the free troposphere, and a longer O<sub>3</sub> lifetime allowing for a longer transport distance than in summer when O<sub>3</sub> production and loss (both chemical and depositional) are largest [Wang *et al.*, 1998; Jaffe *et al.*, 1999; Yienger *et al.*, 2000; Bey *et al.*, 2001; Wild and Akimoto, 2001; Stohl *et al.*, 2002; Liu *et al.*, 2003; Weiss-Penzias *et al.*, 2004; Wild *et al.*, 2004; Liu *et al.*, 2005; Holzer *et al.*, 2005; Holloway *et al.*, 2008]. Over all regions, the summed responses to 20% decreases in anthropogenic NO<sub>x</sub> emissions from all three foreign regions are largest in boreal spring and fall to early

winter (up to ~0.4 ppb); the response to NMVOC emissions in the three foreign regions is largest in winter through early spring (0.2–0.4 ppb). Over NA, the model ensemble average O<sub>3</sub> response to NO<sub>x</sub> and NMVOC emissions in the three foreign regions are similar (~0.3 ppb) in winter, spring and summer, although this result varies across models (section 4.3). The 20% reductions of CO emissions in the three foreign regions have little influence (<0.2 ppb) on surface O<sub>3</sub> over the receptor regions, but this influence increases when the long-term feedback via CH<sub>4</sub> is included (section 5.2).

[21] In Figure 6, we decompose the foreign impact in the “ALL” simulations into the contributions from each of the three foreign source regions. For the NA receptor region, EA and EU contribute similarly from April through November.



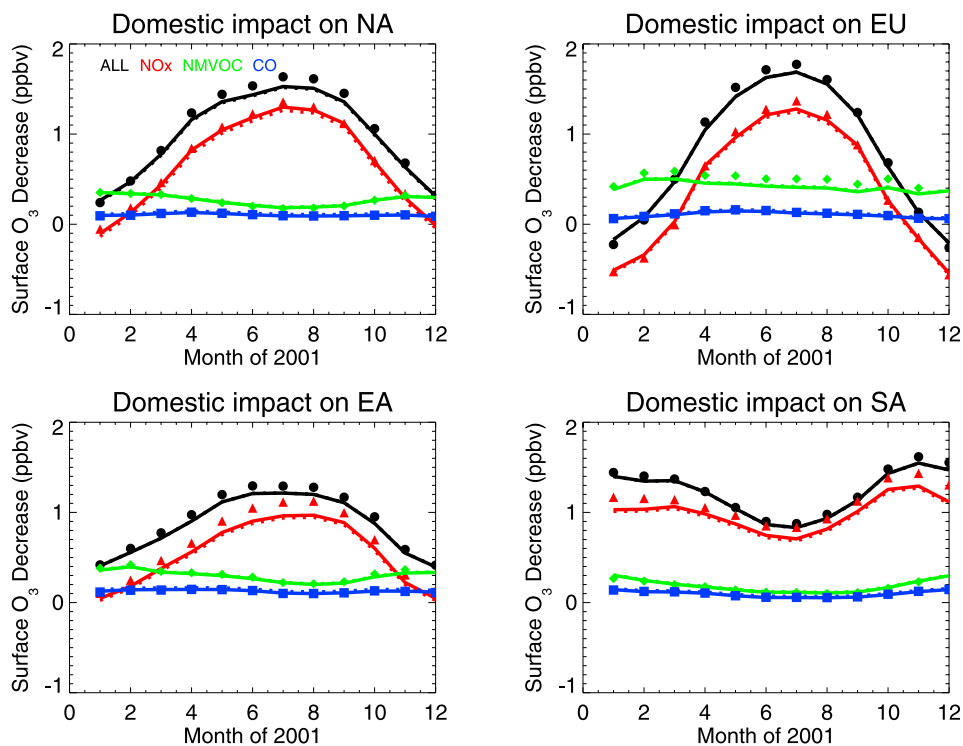


**Figure 4.** Decrease in monthly mean surface O<sub>3</sub> over the receptor regions (one per plot) resulting from 20% reductions in anthropogenic O<sub>3</sub> precursor emissions within the same region: NO<sub>x</sub> (SR1–SR3; red), NMVOC (SR1–SR4; green), CO (SR1–SR5; blue), and combined (ALL; SR1–SR6; black). Model ensemble means are shown for all available model results (solid symbols; see auxiliary material Data Set S4 for the number of models contributing to each simulation) and for the subset of models in Table 2 (solid lines). The dotted lines show the model ensemble mean total O<sub>3</sub> response for the models in Table 2 (using all available simulations although not all models conducted every simulation) after accounting for the long-term impact from changes in CH<sub>4</sub> (see section 5.2 for details) and show little change from the short-term results.

NA contributes most strongly to EU throughout the year, reflecting its upwind proximity. The SA source region exerts a minor influence throughout the year on surface O<sub>3</sub> over NA and EU (always less than 0.1 ppb to surface O<sub>3</sub>), as SA pollution is typically funneled away from the northern midlatitude westerlies (the dominant transport pathway to those regions) [e.g., *Li et al.*, 2001; *Lelieveld et al.*, 2002a; *TF HTAP*, 2007], and tends to remain isolated from midlatitude air [*Bowman and Carrie*, 2002; *Hess*, 2005]. Over EA, emissions from the three foreign source regions induce a similar response in surface O<sub>3</sub> during summer, with stronger sensitivity to emissions in EU (followed by NA) during spring, and to NA (followed by EU) in winter. Over SA, the surface O<sub>3</sub> response is largest when emissions are reduced in EU, except for the November peak which is driven by emissions from EA. For part of the year, surface O<sub>3</sub> over the receptor regions is similarly influenced by at least two foreign source regions, except for EU which is always influenced most by NA.

[22] In order to compare the surface O<sub>3</sub> response to emission reductions in the three foreign regions versus the domestic region, we define a regional “import sensitivity” (IS<sub>r</sub>),

$$IS_r = \left( \sum_{f=1}^3 \Delta O3_{fr} \right) / \Delta O3_{rr},$$

where IS<sub>r</sub> represents the import sensitivity for receptor region *r*; ΔO3<sub>fr</sub> represents the model ensemble mean change in surface O<sub>3</sub>, spatially averaged over the receptor region *r*, produced by a 20% decrease in anthropogenic emissions over the foreign source region (*f*); ΔO3<sub>rr</sub> is the change in surface O<sub>3</sub> resulting from the 20% reduction of anthropogenic emissions within the domestic source region. The larger the value of the import sensitivity, the greater the relative influence of emissions from the three foreign regions. Note that the import sensitivity neglects the influence of foreign emissions in regions not considered here, and is unlikely to be representative of the relative importance of foreign versus domestic emission changes in urban airsheds not resolved by global models. Nevertheless, this metric enables us to gauge the large-scale O<sub>3</sub> responses to foreign versus domestic emission changes, and how their relative importance varies by region and season.

[23] The annual mean IS<sub>r</sub> ranges from approximately 0.3 (NA and SA) to 0.7 (EU) for NO<sub>x</sub> alone; 0.4 (EU) to 1.1 (SA) for NMVOC alone; and 0.5 (NA and SA) to 0.7 (EU) for the combined reductions in all O<sub>3</sub> precursors. The IS<sub>r</sub> for CO ranges from approximately 0.8 (EA) to 1.2 (EU), reflecting the longer CO lifetime and the correspondingly smaller influence from domestic sources. Monthly mean IS<sub>r</sub> estimates from the ALL simulations are shown in Figure 7. Over EA, NA, and EU, IS<sub>r</sub> exceeds 1 during boreal winter (also in early

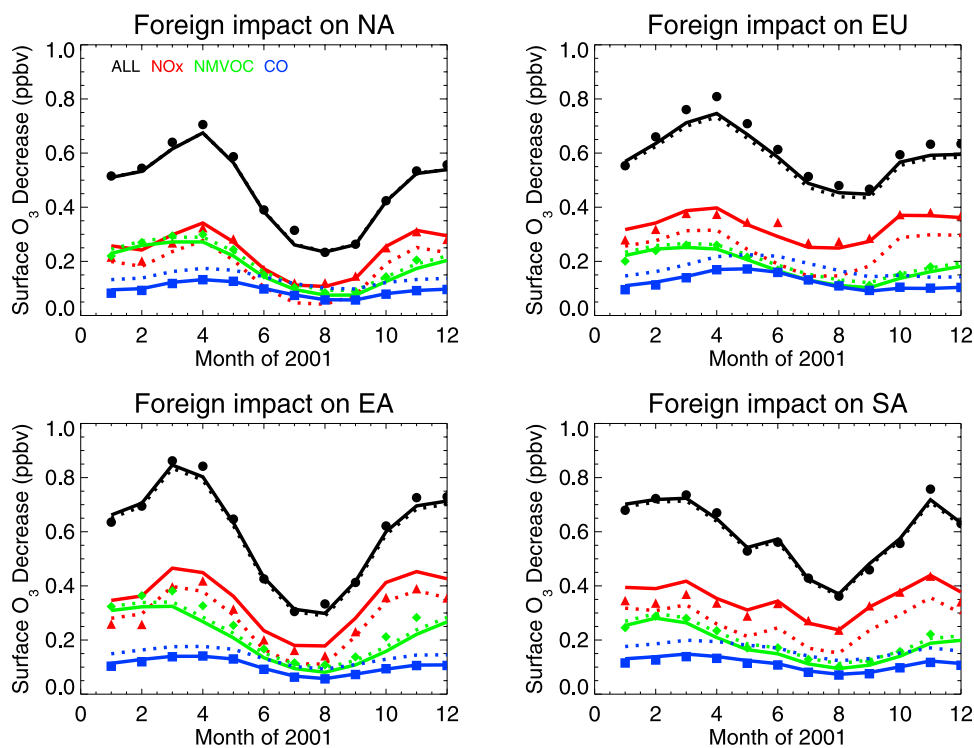


**Figure 5.** The sum of the monthly mean surface  $O_3$  decreases over the receptor regions (one per plot) in the three simulations in which anthropogenic emissions were reduced by 20% in the foreign source regions:  $NO_x$  (SR1–SR3; red), NMVOC (SR1–SR4; green), CO (SR1–SR5; blue), and combined (ALL; SR1–SR6; black). As in Figure 4, the model ensemble means are shown for all available model results (solid symbols), for the subset of models in Table 2 (solid lines), and for the total  $O_3$  response estimated after accounting for the long-term impact from changes in  $CH_4$  using the models in Table 2 (dotted lines). Note that a change in scale from Figure 4 is necessary for the ordinate axis since the responses to foreign emissions are smaller.

spring and late fall over EU) when the  $O_3$  response to domestic emissions is small (Figure 4). Even in summer, when domestic  $O_3$  production peaks,  $IS_r$  is 0.2–0.3 over these regions. During the month with the largest absolute surface  $O_3$  response to ALL emission reductions in the three foreign regions (Figure 6),  $IS_{NA} = 0.6$  (April),  $IS_{EU} = 0.7$  (April), and  $IS_{EA} = 1.1$  (March). The  $IS_{SA}$  for ALL varies little during the year (Figure 7) and is  $\sim 0.5$  in November and during the broad secondary peak of influence from the three foreign regions from January through April (Figure 6). We conclude that the  $O_3$  response to emissions in the three foreign regions is not negligible when compared to the response to domestic emissions, and is particularly strong in spring and fall at northern midlatitudes.

#### 4.2. Applicability of Results to Other Emission Perturbations

[24] Evaluating whether the  $O_3$  response to multicomponent emission reductions is equivalent to the sum of the responses to single component emission reductions is critical for determining the applicability of our results to other combinations of precursor emission reductions. In order to assess the additivity of our simulations, we construct the ratio of the sum of the  $O_3$  response to 20% reductions in emissions of the individual precursors  $NO_x$ , NMVOC, and CO, i.e.,  $(SR3 - SR1) + (SR4 - SR1) + (SR5 - SR1)$  to the  $O_3$  response in the

simulation where all precursors (along with aerosols) were reduced simultaneously (SR6–SR1). With one exception, models including reductions of aerosols and aerosol precursors in SR6 indicate that the sum of the responses to single component emission reductions exceeds that to multicomponent perturbations, by as much as 50% for some SR pairs (auxiliary material Data Set S5 and Figure S3). The degree of additivity varies by region within individual models (auxiliary material Figure S3). In Figure 8, we restrict our analysis to those models without aerosol changes in SR6, and find that the summed surface  $O_3$  responses to single-component emission reductions are approximately equivalent to those from multicomponent reductions for emission changes in the domestic and the three foreign source regions combined. We conclude that combined reductions in emissions of aerosols and  $O_3$  precursors dampen the  $O_3$  response relative to that produced by emission reductions of the  $O_3$  precursors alone. Only two out of six of these models include feedbacks of aerosol changes on photolysis rates (auxiliary material Data Set S5), so this damping effect must operate primarily through chemical interactions in the models, for example by reducing aerosol uptake of  $O_3$  precursors.

[25] If we wish to apply the responses diagnosed in section 4.1 more broadly, we need to determine if the  $O_3$  response is sufficiently linear to yield accurate results when scaling to emission perturbations of other magnitudes. To

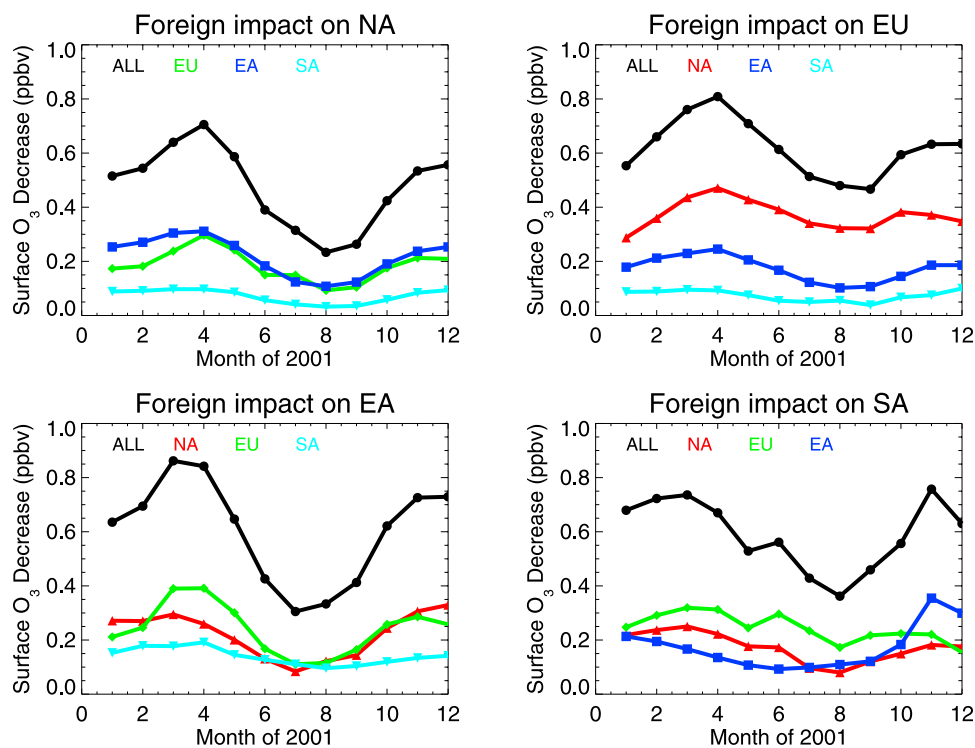


**Figure 6.** Decrease in the 15-model ensemble monthly mean surface  $O_3$  over the receptor regions (one per plot) resulting from simultaneous 20% decreases in all anthropogenic  $O_3$  precursor emissions in the three foreign source regions combined (ALL; black line with circles) and individually: NA (red line with triangles), EU (green line with diamonds), EA (dark blue line with squares), and SA (cyan line with inverted triangles) as determined from the difference of the SR1 and SR6 simulations. The black line with circles (ALL) is identical to the black circles in Figure 5.

address this point, additional simulations with varying sized perturbations to EU anthropogenic  $NO_x$  emissions were conducted in the FRSGC/UCI model [Wild *et al.*, 2003]. The FRSGC/UCI model tends to produce a larger surface  $O_3$  response to  $NO_x$  than the model ensemble mean, but is not an outlier in any month, so we expect these results to apply generally to our model ensemble. Figure 9 shows the response of surface  $O_3$  over EU and NA. The EU source region was chosen as it exhibits the most nonlinear response of all regions (e.g., reversing sign with season in Figure 4). The response over the source region (EU) deviates more from that obtained by a linear scaling of the response in the 20% perturbation simulation than over a remote receptor region (NA). For example, the summertime response over the EU remains linear only for perturbations within 20%, whereas it is fairly linear well beyond perturbations of 50% over NA. The response is most linear in summer over the foreign receptor region. A companion manuscript (Wu *et al.*, submitted manuscript, 2009) expands this analysis by incorporating simulations from other models, perturbations to other  $O_3$  precursor emissions and in other source regions.

#### 4.3. Robustness of Results as Measured by Intermodel Differences

[26] We first examine whether the surface  $O_3$  bias versus observations in the individual models over the eastern United States (section 3) manifests as a larger response, for example, of EU surface  $O_3$  to the reductions in NA emissions. We find little correlation between the bias and the simulated SR

relationships ( $r^2 < 0.1$  for the EU response to NA emission changes in July). The source of the bias, however, requires further investigation to increase confidence in the estimates for summertime SR relationships for the NA and EA regions.

[27] We next interpret the model range of  $O_3$  responses to emission changes as a measure of the combined uncertainty from differences in the emission inventories and the representations of transport and photochemical processes in the individual models. The model spread (measured by the relative standard deviation,  $\sigma/\mu$ ) associated with the  $O_3$  response to decreases in NMVOC emissions is often larger than that due to reductions in either  $NO_x$  or CO emissions (auxiliary material Data Set S4), and probably reflects the larger uncertainty associated with the NMVOC inventories and the incorporation of the individual NMVOC species into the model chemical mechanisms (Table 1). For example, Figure 10 shows that the magnitude of the surface  $O_3$  response over NA to decreases in EU anthropogenic NMVOC emissions in the individual models correlates ( $r^2 = 0.50$ ) with the anthropogenic EU NMVOC emission total, which varies by nearly a factor of 10. Although Figure 5 suggests that surface  $O_3$  over NA has a similar sensitivity to emissions of  $NO_x$  and NMVOC in the three foreign regions, this result varies across the models (not shown). Better constraints on the total NMVOC emissions and their partitioning into NMVOC species with different reactivity should help to reduce the associated uncertainty in the  $O_3$  sensitivity.

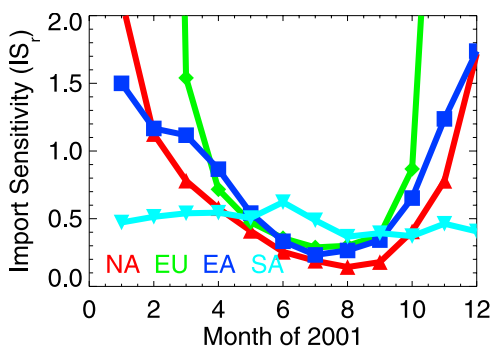


**Figure 7.** Monthly mean import sensitivities for each region ( $IS_r$ ; where  $r = \text{NA}$  (red), EU (green), EA (blue), and SA (cyan)) for the simulations with simultaneous 20% decreases in anthropogenic  $\text{NO}_x$ , CO, and NMVOC emissions (ALL), calculated as described in section 4.1. Not shown are the values  $> 2$  for  $IS_{\text{NA}}$  (December and January) and  $IS_{\text{EU}}$  (November and February) which result from the small wintertime domestic responses, nor the negative values for  $IS_{\text{EU}}$  (December and January) which result from  $\text{O}_3$  titration by EU  $\text{NO}_x$  emissions (see domestic responses in Figure 4).

[28] For each region, we assess the robustness of the SR relationships in Figure 6 across the 15 individual models. We focus here on the springtime (March, April and May) response to the combined emissions reductions (i.e., SR6–SR1; auxiliary material Figure S2). The rankings for the EU receptor region are most robust, with  $\text{NA} > \text{EA} > \text{SA}$  in all models. All models also indicate that springtime  $\text{O}_3$  over EU and NA is less sensitive to emissions from SA versus the other two foreign regions. The model spread in the

response of NA surface  $\text{O}_3$  to emission reductions in EU versus EA in spring indicates more uncertainty, with 10 models predicting equivalent responses (to within 20%), but in four models the response to EA emissions is 30–55% greater than that to EU emissions. Over EA, where the winds are northwesterly during spring, the  $\text{O}_3$  response to emission changes in EU and NA exceeds that to SA (by a factor of 1.6–3 for EU in 12 models, and 1.5–2 for NA in 9 models). Over SA, the  $\text{O}_3$  response to emission changes rank as  $\text{EU} > \text{NA} > \text{EA}$  in 9 of 15 models for spring. Future work should investigate why some models respond differently from the majority, and the relative roles of emissions, transport, and chemistry in contributing to these differences. Priority should be placed on identifying observation-based constraints that can be used to select those models that most accurately represent the key processes contributing to hemispheric ozone transport.

#### 4.4. Comparison With Prior Estimates of Intercontinental Source-Receptor Relationships

[29] In Figure 11, we compare our results for the NA, EU, and EA regions with the studies referenced by *TF HTAP* [2007] that report annual and seasonal mean SR relationships, supplemented by recent analyses by *Lin et al.* [2008], *Duncan et al.* [2008], and *Holloway et al.* [2008]. While the range across previous studies reflects a variety of regional definitions, reported metrics, meteorological years, and methods for source attribution, the consistent modeling approach adopted here restricts the range across our model results to differences in emissions, chemistry, transport, and resolution (both horizontal and vertical). Information regarding import to or export from the SA region is limited; our results in Figure 5 for SA are consistent with those of *Kunhikrishnan et al.* [2006] in showing an autumn peak, but in contrast to

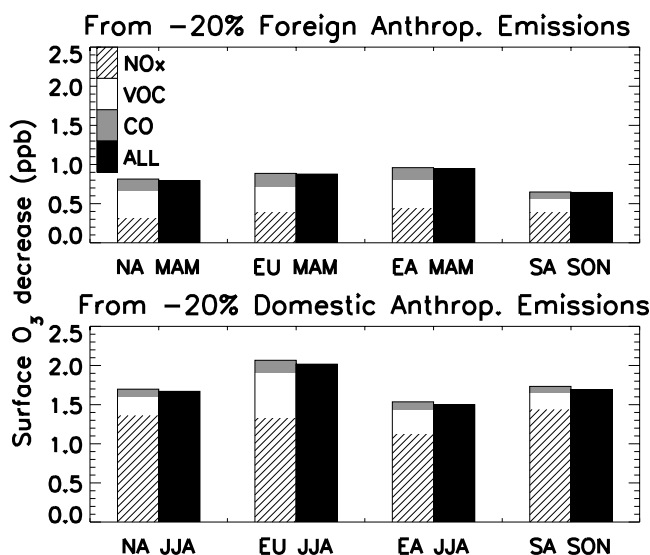


**Figure 8.** Multimodel spatial average decrease in surface  $\text{O}_3$  over the receptor regions resulting from 20% reductions in the  $\text{O}_3$  precursor emissions in the (top) three foreign and (bottom) domestic source regions for the season of peak sensitivity to those emissions (determined from Figures 5 and 4, respectively) in those models where aerosol emission reductions are not included in the SR6 simulation (FRGSC/UCI, GEMAQ-v1p0, STOC-HadAM3-v01, and UM-CAM-v01). Each shaded region in Figure 8 (top) represents a summation of the model ensemble mean surface  $\text{O}_3$  responses to the emission perturbations in the three foreign source regions.

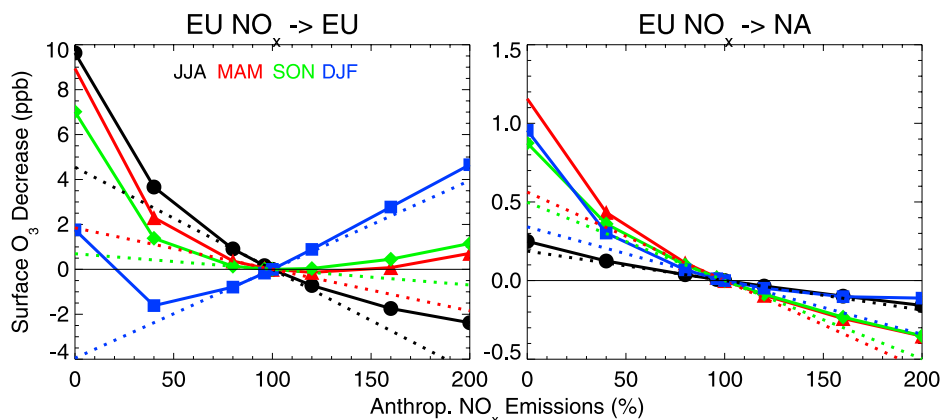


**Figure 9.** Change in spatial average surface  $O_3$  over the (left) EU and (right) NA as a function of various size perturbations to EU anthropogenic  $NO_x$  emissions by season (colors), as simulated with the FRSGC/UCI model (solid lines with symbols) and as estimated by scaling linearly from the response in the simulation where  $NO_x$  emissions were decreased by 20% (SR1–SR3EU; dotted lines).

that study, we find that the response of SA surface  $O_3$  to EA  $NO_x$  emissions is larger in winter than in summer.

[30] For previous studies in which the  $O_3$  response was examined for emission perturbations smaller than 100%, we scale the reported results linearly to estimate the total contribution from foreign anthropogenic emissions. To compare our model results with prior studies, we scale our responses diagnosed for 20% emission decreases to 100% by using  $5 \times$  (SR1 – SR6) to estimate the total contribution of anthropogenic  $NO_x + NMVOC + CO$  emissions in a foreign source region to surface  $O_3$  in a receptor region. Figure 10 implies that a linear scaling of our 20% reductions in anthropogenic  $NO_x$  emissions will yield a smaller response than in a simulation where emissions are set to zero. The response to the combined  $NO_x + NMVOC + CO$  emission reductions should deviate less from linearity owing to competing effects on OH from  $NO_x$  versus  $NMVOC+CO$  but this assumption needs further investigation. The range in annual mean SR relationships for the EU and EA receptor regions across our model ensemble narrows considerably from the estimates in the literature, with the model ensemble response in Figure 11 smaller than most prior estimates for spring and summer. Our study provides a comprehensive view of the seasonality of SR relationships and a previously unavailable quantitative measure of intermodel spread which may indicate uncertainty in these relationships.

## 5. Contribution From $CH_4$ to the Long-Term Response of $O_3$

### 5.1. Surface $O_3$ Response to $CH_4$ Concentrations

[31] The ensemble annual mean surface  $O_3$  response to a 20% decrease in global  $CH_4$  concentrations is 1.1–1.3 ppb averaged over the receptor regions, largest in SA and EU, followed by NA and EA (auxiliary material Data Set S4). The  $O_3$  responses in the individual models, however, differ by  $\sim 1$  ppb (ranging from 0.7 to 1.6 ppb over EA; 0.8 to 1.8 over EU; 0.8 to 1.7 over NA; 0.9 to 1.8 over SA). This range likely reflects model differences in OH and  $NO_x$  distributions [e.g., Fiore *et al.*, 2008]. Since the  $O_3$  response to  $CH_4$  is approximately linear over the range of present-day anthropogenic emissions [Fiore *et al.*, 2008], we can scale the

ensemble mean responses in auxiliary material Data Set S4 from 20% to 100% to estimate that  $CH_4$  presently contributes 5.5–6.5 ppb to surface  $O_3$  in the receptor regions, consistent with the multimodel estimate of Prather *et al.* [2001] that anthropogenic  $CH_4$  ( $\sim 60\%$  of the global total) contributes 4 ppb to surface  $O_3$ .

[32] The stronger  $O_3$  response to  $CH_4$  over SA is consistent with its tropical location where OH is abundant and the temperature-sensitive  $CH_4$ -OH reaction proceeds faster [e.g., Spivakovsky *et al.*, 2000]. One might then expect that EU, situated at more northerly latitudes than the other regions, would exhibit the weakest response of surface  $O_3$  to  $CH_4$ . Instead, the response is nearly as strong as that found in SA, and stronger than the responses in NA and EA. The largest peak-to-peak amplitude of the  $O_3$  response to  $CH_4$  occurs in EU, followed by SA, NA, and EA (auxiliary material Figure S4). The  $O_3$  response to  $CH_4$  over EU is largest during summer, possibly reflecting a combination of the stronger seasonality in  $O_3$  production in this northern region and stronger  $CH_4$  sensitivity arising from smaller biogenic

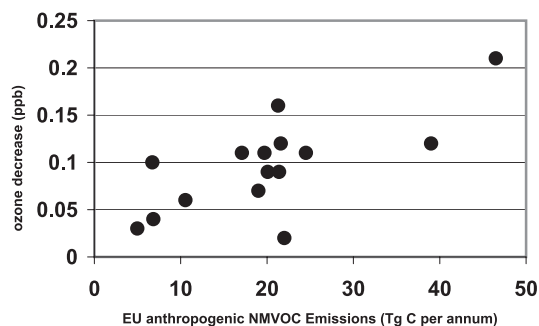


**Figure 10.** Decrease in annual spatial mean NA surface  $O_3$  (ppb) resulting from 20% reductions in EU anthropogenic NMVOC emissions (SR1–SR4EU) plotted against the EU anthropogenic NMVOC emissions ( $Tg\ C\ a^{-1}$ ). The points represent the results from individual models. EU anthropogenic NMVOC emissions are given in auxiliary material Data Set S3 for each model. The coefficient of determination ( $r^2$ ) is 0.50.

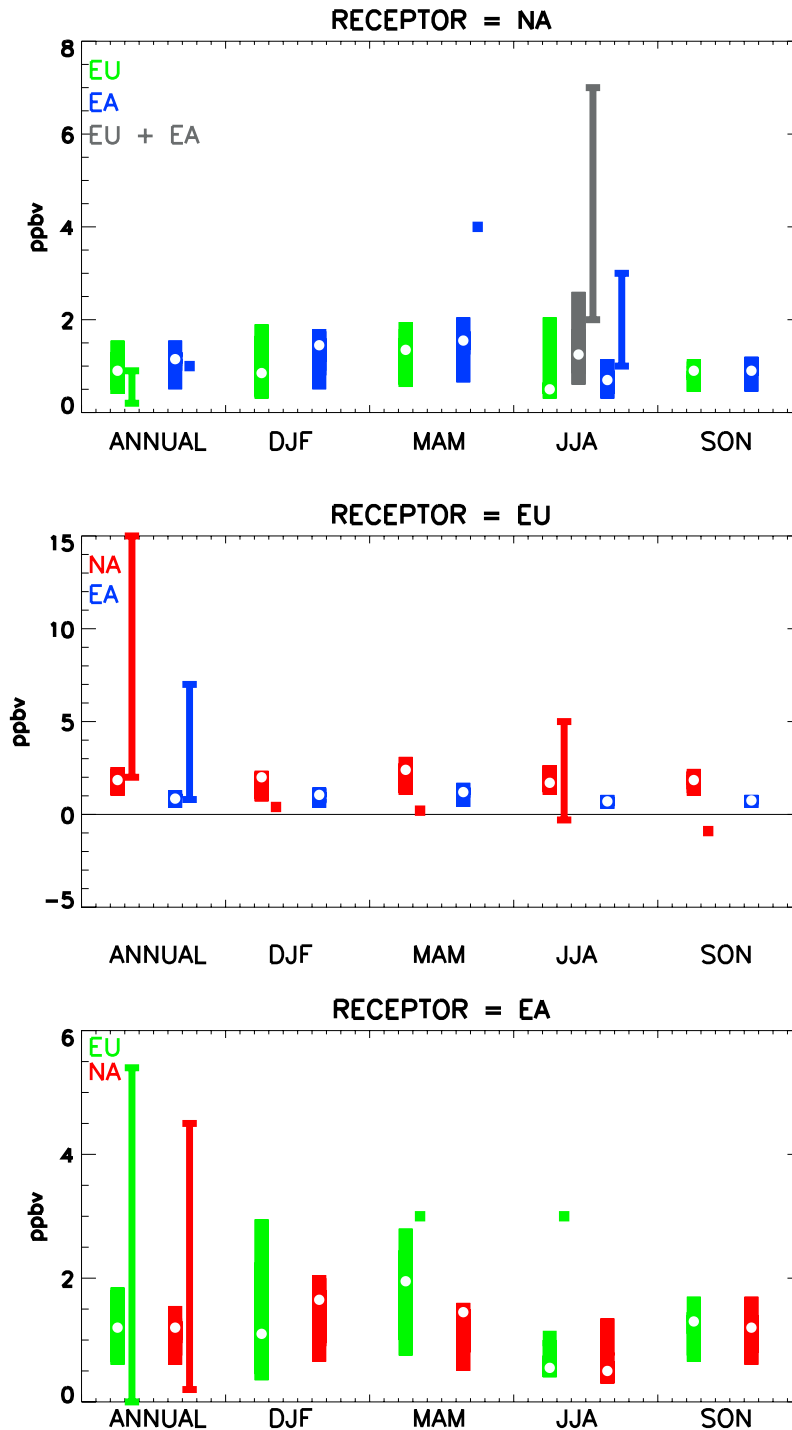


**Figure 11.** Annual and seasonal mean contribution to total surface  $O_3$  from foreign source regions as estimated from the individual model results in this study (colored by source region: green for EU, blue for EA, gray for EA + EU, and red for NA) and from studies in the published literature (thin vertical bars for ranges across studies and regions; squares where one value is reported; note that regional definitions, methods for source attribution, and reported metrics (e.g., 24-h versus afternoon versus daytime mean) vary across studies) [Derwent *et al.*, 1998; Berntsen *et al.*, 1999; Wild and Akimoto, 2001; Derwent *et al.*, 2002; Fiore *et al.*, 2002b; Jaeglé *et al.*, 2003; Li *et al.*, 2002; Liu *et al.*, 2002; Pochanart *et al.*, 2003; Derwent *et al.*, 2004; Wild *et al.*, 2004; Auvray and Bey, 2005; Guerova *et al.*, 2006; Sudo and Akimoto, 2007; Duncan *et al.*, 2008; Holloway *et al.*, 2008; Lin *et al.*, 2008]. All results are scaled to 100% contributions as in Table 5-2 of *TF HTAP* [2007]. The contributions from this work are estimated by linearly scaling the simulated surface  $O_3$  response to the combined 20% decreases in anthropogenic emissions of  $NO_x$ , CO, and NMVOC in the foreign source regions to 100% decreases, i.e.,  $5 \times (SR1 - SR6)$ . The white circles represent the multimodel median value.

(high reactivity) VOC emissions than in the other regions. The seasonal amplitude of the EU O<sub>3</sub> response to CH<sub>4</sub> in the individual models is indeed somewhat correlated with the ratio of EU anthropogenic to total NMVOC emissions ( $r = 0.7$  for 15 models).

## 5.2. Long-Term O<sub>3</sub> Response to NO<sub>x</sub>, CO, and NMVOC Emissions Reductions

[33] Perturbations to NO<sub>x</sub>, CO, and NMVOC emissions influence the oxidizing capacity of the atmosphere (OH), which can change the CH<sub>4</sub> lifetime and thereby contribute a “long-term” change in tropospheric O<sub>3</sub> on the decadal timescale of the CH<sub>4</sub> perturbation lifetime [e.g., Prather, 1996; Daniel and Solomon, 1998; Fuglestedt et al., 1999; Wild and Prather, 2000; Derwent et al., 2001; Wild et al., 2001; Collins et al., 2002; Stevenson et al., 2004]. Using the method described below, West et al. [2007] previously found that the long-term impacts of 20% decreases in global anthropogenic emissions on population-weighted average surface O<sub>3</sub> at northern midlatitudes enhanced the short-term response by 16–21% for CO, and decreased it by 6–14% for NO<sub>x</sub>, with little long-term influence from NMVOC. This long-term impact on surface O<sub>3</sub> exhibits the spatial distribution of the surface O<sub>3</sub> response to changes in CH<sub>4</sub>, which we obtain here from the difference in O<sub>3</sub> between the SR2 and SR1 simulations for each model (section 5.1). By setting atmospheric CH<sub>4</sub> to a uniform, fixed value of 1760 ppb, the SR3 through SR6 simulations neglect the feedback on CH<sub>4</sub> from the changes in OH induced by the 20% decreases in regional anthropogenic NO<sub>x</sub>, NMVOC, and CO emissions. In order to account for this feedback, we first estimate what the steady state CH<sub>4</sub> concentration change would be in a simulation in which CH<sub>4</sub> concentrations were allowed to respond to OH changes, but with CH<sub>4</sub> emissions held equal to those implied by the 1760 ppb atmospheric abundance in SR1. The treatment of CH<sub>4</sub> as a uniform, fixed value should not introduce any error in the estimated O<sub>3</sub> response to changes in CH<sub>4</sub> since the spatial distribution of the O<sub>3</sub> response to CH<sub>4</sub> has been shown to be identical (spatial correlation of  $r = 1.0$ ) in a full transient CH<sub>4</sub> simulation (i.e., with CH<sub>4</sub> varying spatially) and in a simulation with CH<sub>4</sub> set to a globally uniform, fixed value [Fiore et al., 2008].

[34] We apply the formulation of West et al. [2007] to estimate the CH<sub>4</sub> abundance that would result from the changes in the other O<sub>3</sub> precursor emissions,

$$[\text{CH}_4]_{\text{SRNxx}} = [\text{CH}_4]_{\text{SR1}} \times (\tau_{\text{SRNxx}}/\tau_{\text{SR1}})^F,$$

where SRN represents SR3 through SR6; xx is the two-letter regional abbreviation in Figure 1;  $\tau_{\text{SR1}}$  is the total atmospheric CH<sub>4</sub> lifetime (assuming CH<sub>4</sub> losses to soils and the stratosphere with lifetimes of 160 and 120 years [Prather et al., 2001], respectively). in the base simulation;  $\tau_{\text{SRNxx}}$  is the CH<sub>4</sub> lifetime in the perturbation simulation; and F is defined as the ratio of the atmospheric response (perturbation) time to the global atmospheric lifetime (see below). Table 2 lists the subset of models that archived the CH<sub>4</sub> loss rates required to determine  $\tau_{\text{SR1}}$ ,  $\tau_{\text{SRNxx}}$ , and F. The model ensemble mean  $\tau_{\text{SR1}} = 8.55 \pm 1.6$  is within 2% of the 26-model mean of  $8.67 \pm 1.32$  reported by Stevenson et al. [2006], and the ensemble mean methane lifetime against loss by tropospheric OH of  $10.2 \pm 1.7$  agrees well with observationally

**Table 2.** Methane Lifetime and “Feedback Factor” in the Individual Models<sup>a</sup>

Model	$\tau_{\text{OH}}^b$	$\tau_{\text{tot}}^c$	F <sup>d</sup>
CAMCHEM-3311m13	11.86	10.11	1.30
FRSGUCUI-v01	8.70	7.72	1.43
GISS-PUCCINI_modelE	10.88	9.39	1.36
GMI-v02f	10.38	9.02	1.31
LMDz3-INCA1	10.02	8.74	1.31
LLNL_IMPACT-T5a	6.19	5.68	1.40
MOZARTGFDL-v2	10.44	9.06	1.31
MOZECH-v16	11.20	9.63	1.29
STOC-HadAM3	9.31	8.20	1.31
STOCHEM-HadGEM	11.72	10.01	1.28
TM5-JRC-cy2-ipcc-v1	9.02	7.97	1.43
UM-CAM-v01	12.50	10.57	1.25
Model ensemble mean	10.19	8.84	1.33
Standard deviation	1.72	1.33	0.06

<sup>a</sup>Methane lifetime,  $\tau$ ; feedback factor, F.

<sup>b</sup>The CH<sub>4</sub> lifetime against loss by tropospheric OH (years), defined as the total atmospheric burden divided by the tropospheric CH<sub>4</sub> loss rates, with the troposphere defined using the 150 ppb O<sub>3</sub> chemical tropopause.

<sup>c</sup>The total atmospheric CH<sub>4</sub> lifetime (years) determined from  $\tau_{\text{OH}}$  and assuming CH<sub>4</sub> losses to soils and the stratosphere with lifetimes of 160 and 120 years [Prather et al., 2001], respectively.

<sup>d</sup>The feedback factor is the ratio of the atmospheric response (or perturbation) time to the global atmospheric lifetime and is given by  $1/(1-s)$  where  $s$  is determined from the SR2 and SR1 simulations, and defined as  $(\delta \ln(\tau))/(\delta \ln[\text{CH}_4])$  [Prather et al., 2001], where  $[\text{CH}_4] = 1760$  ppb in SR1 and 1408 ppb in SR2.

derived (from methyl chloroform) estimates of  $10.2^{+0.9}_{-0.7}$  [Prinn et al., 2005]. From the SR1 and SR2 simulations, we calculate F following Wild and Prather [2000],

$$F = 1/(1-s)$$

$$s = (\ln(\tau_{\text{SR2}}) - \ln(\tau_{\text{SR1}}))/(\ln(B_{\text{SR2}}) - \ln(B_{\text{SR1}})),$$

where  $B$  is the total atmospheric CH<sub>4</sub> burden.  $F$  describes the response of the atmospheric CH<sub>4</sub> abundance to a change in CH<sub>4</sub> emissions. In the case of a small perturbation,  $F$  is approximately the ratio of the relative change in CH<sub>4</sub> concentrations to an imposed emission change. For example, the model ensemble mean  $F$  of 1.33 (Table 2) implies that a 1% increase in CH<sub>4</sub> emissions would ultimately yield a 1.33% increase in CH<sub>4</sub> concentrations. The multimodel mean  $F$  is at the low end of the reported range of 1.33–1.45 range (and within 10% of the recommended value of 1.4) by Prather et al. [2001].

[35] Following Naik et al. [2005] and West et al. [2007], we estimate the long-term impact on O<sub>3</sub> by scaling linearly the change in surface O<sub>3</sub> in the CH<sub>4</sub> perturbation simulation (SR2–SR1) for each model grid cell by the ratio of the estimated changes in CH<sub>4</sub> from SR1 to SRNxx versus SR2,

$$\Delta\text{O}_3(\text{SRNxx} - \text{SR1})$$

$$= [\Delta\text{CH}_4(\text{SRNxx} - \text{SR1})/\Delta\text{CH}_4(\text{SR2} - \text{SR1})]$$

$$\times \Delta\text{O}_3(\text{SR2} - \text{SR1}).$$

For each model, we then calculate the domain average “long-term” O<sub>3</sub> response for each region in Figure 1 and add this  $\Delta\text{O}_3$  to the short-term O<sub>3</sub> response (averaged over each region) diagnosed directly from SRNxx-SR1.

[36] Including the long-term feedback through CH<sub>4</sub> has little impact on the model ensemble mean domestic response

(solid versus dotted lines in Figure 4). In contrast, a larger percentage change occurs for the  $O_3$  response to emissions in foreign regions since the  $O_3$  response to changes in  $CH_4$  (SR2–SR1) is relatively uniform globally. Figure 5 shows that the long-term contribution partially offsets the estimated  $O_3$  decrease from  $NO_x$  emission reductions within the three foreign regions, since the net global effect of decreasing surface  $NO_x$  emissions is to lower OH, causing the  $CH_4$  abundance to rise, thereby enhancing the  $CH_4$  contribution to surface  $O_3$ . During the month of maximum contribution from the three foreign regions (April for NA, EU, and EA and November for SA), the long-term effect reduces the short-term  $O_3$  decrease by  $\sim 15$ –20%. During the same months, the short-term  $O_3$  responses to the 20% reductions in CO and NMVOC emissions from the three foreign regions are augmented by 30–40% and  $\sim 10\%$ , respectively, since decreasing CO or NMVOC increases OH. These results are qualitatively consistent with those of *West et al.* [2007]. Over NA and EU during summer, the opposing influences of the long-term feedback from  $NO_x$  and CO result in the total impact of the CO emission reductions exceeding that from  $NO_x$  (or NMVOC). As there is little seasonality in the  $O_3$  response to  $CH_4$  (SR2–SR1), the seasonal cycle of the total  $O_3$  response is mainly driven by the short-term response to the changes in  $NO_x$ , CO, and NMVOC emissions (Figure 5).

[37] In the case of the simultaneous reductions in  $NO_x$ , NMVOC, and CO emissions from all three foreign regions, the long-term feedback is minimal (always less than 3% for all months and regions in Figure 5). The balancing effect of simultaneous changes of  $NO_x$ , CO, and NMVOC has been noted before in the context of the remarkable stability of OH concentrations from the pre-industrial to the present-day atmosphere [*Wang and Jacob, 1998; Lelieveld et al., 2002b*]. Since anthropogenic sources of  $NO_x$ , CO, and NMVOC differ, however, equivalent percentage reductions would not necessarily be applied to all precursors together, in which case the long-term effect should be considered.

### 5.3. Inferring the $O_3$ Response to Regional Reductions in Anthropogenic $CH_4$ Emissions

[38] The results from the simulation in which the global  $CH_4$  abundance was decreased uniformly by 20% are not directly comparable with those from the 20% regional reductions of the other  $O_3$  precursors. In this section we attempt such a comparison by approximating the surface  $O_3$  response that would result from 20% reductions of  $CH_4$  anthropogenic emissions in the source regions.

[39] We first use ensemble mean results to estimate the anthropogenic  $CH_4$  emission decrease that would produce the 20% reduction in global concentrations applied in the SR2 simulation. Applying the model ensemble mean feedback factor (F) of 1.33 from Table 2 (section 5.1) to account for the feedback of  $CH_4$  on its own lifetime, we derive that the 20% decrease in  $CH_4$  abundance corresponds to a 15.4% decrease in total global  $CH_4$  emissions. Assuming that anthropogenic  $CH_4$  emissions are 60% of the total  $CH_4$  emissions [*Denman et al., 2007*], this 15.4% decrease in total global  $CH_4$  emissions corresponds to a 25.7% decrease in global anthropogenic  $CH_4$  emissions. We then use the EDGAR 3.2 FT2000 anthropogenic  $CH_4$  emission inventory [*Olivier et al., 2005*] to estimate that NA, EU, SA, and EA each contribute 16.6%,

16.0%, 17.3%, and 19.0%, respectively, to total global anthropogenic emissions (298 Tg  $CH_4$   $a^{-1}$  in 2000); together the anthropogenic  $CH_4$  emissions from these four regions contribute 68.9% to the global total anthropogenic emissions.

[40] The fraction of the total  $O_3$  response diagnosed from SR2–SR1 that would be produced by 20% decreases in regional anthropogenic  $CH_4$  emissions can then be estimated (i.e., for NA:  $(0.2 \times 16.6\%$  of global anthropogenic emissions)/ $(25.7\%$  decrease in global anthropogenic emissions as implied by the concentration change in SR2)), assuming that the  $O_3$  response scales linearly with changes in the  $CH_4$  burden (which is in turn proportional to changes in emissions over the range of present-day anthropogenic  $CH_4$  emissions [*Fiore et al., 2008*]) and that neither the magnitude of the response nor its spatial pattern depends strongly on the location of the  $CH_4$  emission reductions, as was shown to be the case by *Fiore et al.* [2008]. In this manner, we obtain values of 12.9%, 12.5%, 13.4%, and 14.8% of the  $O_3$  decrease in the SR2 simulation for NA, EU, SA, and EA, respectively. We scale the ensemble mean surface  $O_3$  response to  $CH_4$  over the receptor regions (SR2–SR1 in Table 2) by these values to estimate an annual mean surface  $O_3$  decrease for each SR pair (auxiliary material Data Set S6) that ranges from 0.13 ppb (EU on EA) to 0.20 ppb (EA on SA).

[41] The results are shown in Figure 3 for comparison with the  $O_3$  decreases achieved with reductions in the regional emissions of the traditional  $O_3$  precursors ( $NO_x$ , NMVOC, and CO). While the combined domestic emission reductions of the traditional  $O_3$  precursors (“ALL” in Figure 3) are most effective at reducing surface  $O_3$  over all regions, the additional inclusion of domestic  $CH_4$  emission reductions would yield another 14–20% decrease in annual mean surface  $O_3$ . Comparison of the “3 foreign” bars (black) in “ALL” versus “ $CH_4$ ” in Figure 3 implies that the inclusion of anthropogenic  $CH_4$  emissions in a multispecies control strategy to reduce background surface  $O_3$  in the Northern Hemisphere would nearly double the surface  $O_3$  decrease attained by controlling the traditional  $O_3$  precursors alone. The larger  $O_3$  response over foreign regions to anthropogenic  $CH_4$  versus “ALL”  $O_3$  precursor emissions from SA reflects the comparable amounts of anthropogenic  $CH_4$  emissions from the four regions, whereas SA emits only half as much  $NO_x$  as the other regions. For six SR pairs, regional anthropogenic  $CH_4$  emission reductions are estimated to yield equivalent (within  $\pm 25\%$ ) responses in surface  $O_3$  over foreign continents as the coincident reductions in  $NO_x$ , NMVOC and CO (ALL). For NA on EU and EU on EA, the influence from regional  $CH_4$  emission reductions is roughly half that of the traditional  $O_3$  precursors, and for NA on EA and EU on SA, the  $CH_4$  response is  $\sim 35\%$  less than that to “ALL.” The additional hemispheric-wide  $O_3$  decrease from reductions in anthropogenic  $CH_4$  emissions occurs on the timescale of the  $CH_4$  perturbation time, approximately a decade, whereas the response to the traditional  $O_3$  precursors occurs in weeks to months.

## 6. Response of Air Quality as Measured by Threshold Statistics

[42] In many nations, compliance with air quality standards is assessed with respect to a threshold concentration. *Ellingsen et al.* [2008] have shown that threshold statistics based on 35,



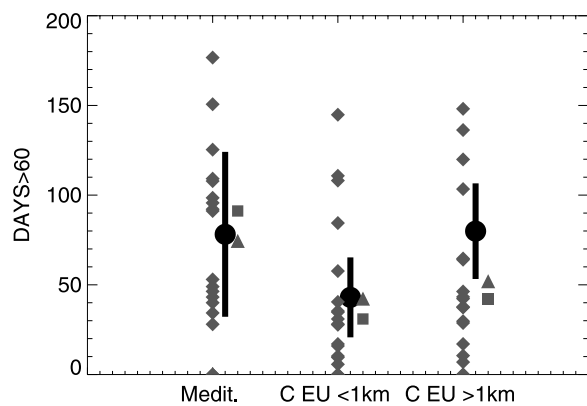


**Figure 12.** Observed (black circles) and simulated (gray diamonds depict results from individual models) annual number of days when daily maximum 8-h average  $O_3$  concentrations exceed 60 ppb at the EMEP stations, averaged over the regions in Figure 2: Mediterranean (Medit.) and central European sites below 1 km altitude (C EU < 1 km) and above 1 km altitude (C EU > 1 km). The black vertical bars depict the standard deviation of the observed values across the stations within the region. The model ensemble mean (gray squares) and median (gray triangles) values from the 18 models that contributed hourly surface  $O_3$  results for SR1 are also shown.

60, and 80 ppb  $O_3$ , simulated by global CTMs, responded similarly to changes in precursor emissions across 14 world regions ( $r^2 > 0.55$ ). Here we focus on incidences of daily maximum 8-h average  $O_3$  concentrations above 60 ppb (DAYS > 60), a statistic used in Europe to protect human health, with a target value of 25 days or fewer per year (e.g., as discussed further by *Ellingsen et al.* [2008]). We previously showed that the model ensemble mean closely matches the monthly average  $O_3$  observations over EU (Figure 2), and so we focus on the EMEP sites (Figure 1) to compare observed and simulated DAYS > 60; results are shown in Figure 12. Over the Mediterranean and low-altitude (below 1 km) central European regions several models (and the model ensemble mean and median) are within the observed range of DAYS > 60. Consistent with the results in Figure 2, Figure 12 shows that the models tend to underestimate DAYS > 60 at high-altitude central Europe with only two models simulating values within the observed range. We recommend further work to determine why some models capture this statistic better than others, including the potential role of differences in mixed layer depths and deposition.

[43] We next explore the relevance of the monthly mean results in Figure 6 for threshold metrics. Figure 13 shows the model ensemble domain average monthly DAYS > 60 in the base simulation (right axis) for each region, and the decrease in these values when all  $O_3$  precursors are reduced by 20% in the four source regions (left axis). In the base simulation, DAYS > 60 peaks in summer over NA and EU, in spring over EA, and in winter to early spring over SA (Figure 13). In all months, DAYS > 60 responds most strongly to the domestic emissions reductions, with  $\sim 20\%$  decreases in DAYS > 60 during the month when the total DAYS > 60 peaks (August for NA, July for EU, May for EA, and March for SA). The response of DAYS > 60 to the foreign

emission reductions is strongest in spring (decreases of 5–10% of the base case for some SR pairs as compared to  $\sim 15$ –35% decreases from domestic emission reductions during the same season). The low incidence of DAYS > 60 in late fall prevents the secondary maximum shown in Figure 6 from emerging. The rankings of the  $O_3$  responses to foreign emission decreases in spring are consistent with those in Figure 6, suggesting that the mean response qualitatively describes the response of the threshold statistics relevant for gauging attainment of air quality standards. We emphasize that the values in Figure 13 are averaged over large spatial areas and mask a large variability within the regions; for example, the model ensemble mean DAYS > 60 over Europe decrease by 2–4 days over much of southern Europe and northern Africa, and by more than 5 days over the Middle East when ALL emissions are decreased by 20% in NA (not shown). A forthcoming manuscript (D. Reidmiller et al., manuscript in preparation, 2009) will expand this analysis to examine variability within the United States.

[44] The annual (spatial average) decrease in DAYS > 60 attained with emission reductions in a foreign region is always  $< 10$ –20% of the decrease from equivalent percentage reductions applied domestically, in contrast to the mean  $O_3$  changes (Figure 3), in which some foreign SR pairs approach 50% of the response to domestic emissions. This result implies that DAYS > 60 (and thus higher  $O_3$  levels) are more sensitive to domestic emissions, with the highest  $O_3$  levels occurring during meteorological conditions favoring regional production from domestic emissions.

## 7. Evaluating the Role of Asian Emission Trends on Northern Midlatitude Surface $O_3$

[45] Observational evidence indicates that background surface  $O_3$  at northern midlatitudes has been increasing by 0.1–0.5 ppb  $a^{-1}$  in recent decades [e.g., *Vingarzan*, 2004; *Carslaw*, 2005; *Jonson et al.*, 2005; *Derwent et al.*, 2007; *Jaffe and Ray*, 2007] although estimated trends vary and may even be leveling off [*Oltmans et al.*, 2006; *Derwent et al.*, 2007]. The model ensemble mean  $O_3$  SR relationships diagnosed here can be combined with reported anthropogenic emission trends to evaluate the role of regional emission changes on Northern Hemispheric background surface  $O_3$ . While wintertime  $O_3$  increases over Europe have been mainly attributed to decreases in EU  $NO_x$  emissions [*Jonson et al.*, 2005; *Ordóñez et al.*, 2005], we focus on the increase observed throughout the year, and examine whether the multimodel ensemble mean SR relationships support the hypothesis that a 0.1–0.5 ppb  $a^{-1}$  increase in Northern Hemispheric background  $O_3$  may be driven by precursor emissions associated with rapid industrialization in Asia [e.g., *Jaffe et al.*, 2003c; *Parrish et al.*, 2004]. Recent satellite retrievals of  $NO_2$  columns suggest that  $NO_x$  emissions from China have increased by  $\sim 40\%$ , with the growth rate accelerating from 4 to 12% per year, from 1996 to 2002 [*Richter et al.*, 2005]. During this same period, little change is found over the United States, while the satellite  $NO_2$  columns suggest a decrease of 30% over western Europe [*Richter et al.*, 2005].

[46] The annual mean surface  $O_3$  response to a 20% decrease in EA anthropogenic  $NO_x$  emissions from auxiliary material Data Set S4 ( $\sim 0.1$  ppb over the foreign regions) implies that a  $+10\% a^{-1}$  increase in EA  $NO_x$  emissions would

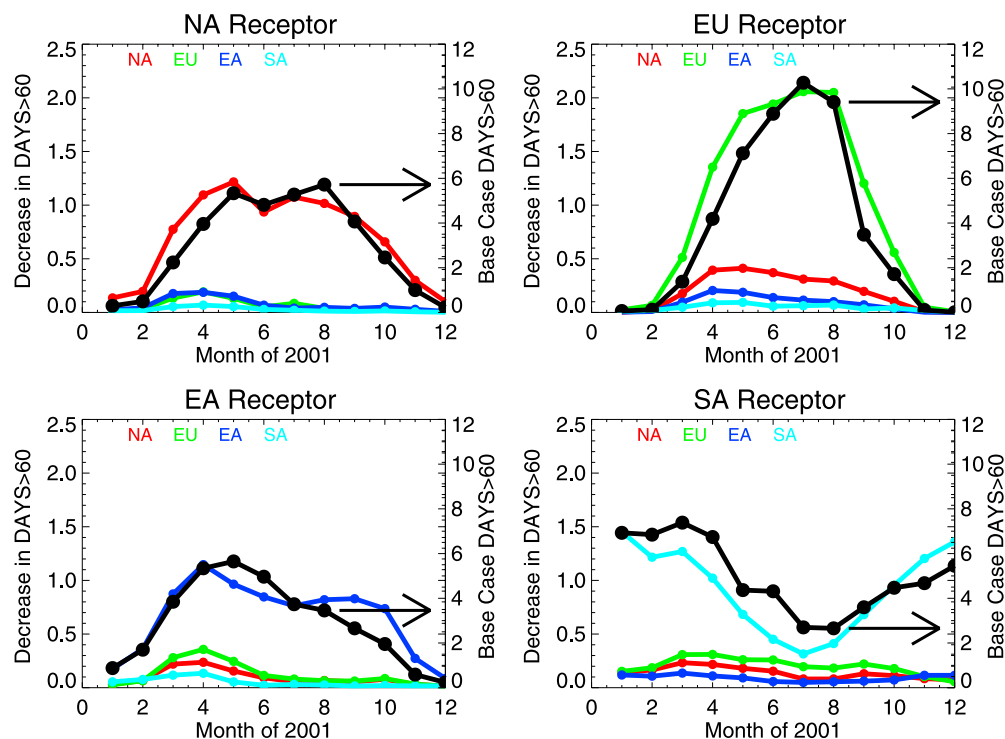


**Figure 13.** Decrease in the model ensemble average number of days per month when daily maximum 8-h average  $\text{O}_3$  concentrations exceed 60 ppb, resulting from simultaneous 20% reductions in anthropogenic  $\text{NO}_x$ , CO, and NMVOC emissions within the source regions (colored lines: red, NA; green, EU; dark blue, EA; light blue, SA), spatially averaged over each receptor region. Also shown are the model ensemble average DAYS > 60 in the base case SR1 simulation for each region (black lines; right axes as indicated by arrows). The change is estimated by first calculating the area-weighted spatial average value for DAYS > 60 in each model simulation for a given region, and then taking the multimodel average of the differences in these spatially averaged DAYS > 60 values (SR1 – SR6). Hourly surface  $\text{O}_3$  values are taken from the SR6 and SR1 simulations in 13 models: CAMCHEM, ECHAM5-HAMMOZ, EMEP, FRSGC/UCI, GEMAQ-v1p0, GEOS-Chem-v07, GMI, LMDz3-INCA1, LLNL-IMPACT, MOZARTGFDL, MOZECH, TM5-JRC-cy2-ipcc, and UM-CAM.

increase  $\text{O}_3$  by  $\sim 0.05 \text{ ppb a}^{-1}$ , below the observed range. If we instead assume that all Asian (i.e., EA + SA) emissions are increasing together with  $\text{NO}_x$ , the 20% emission reductions in Asia produce a  $\sim 0.2$  (over EU) to  $0.3 \text{ ppb}$  (over NA)  $\text{O}_3$  decrease (“ALL” in auxiliary material Data Set S4). In this case, the  $10\% \text{ a}^{-1}$  increase in Asian  $\text{O}_3$  precursor emissions scales to an  $\text{O}_3$  response that falls within the lower end of the surface  $\text{O}_3$  increase derived from observations: an increase of  $0.1$  and  $0.15 \text{ ppb O}_3 \text{ a}^{-1}$ , averaged over the EU and NA receptor regions, respectively. Considering the decreases in European  $\text{NO}_x$  emissions ( $\sim 5\% \text{ a}^{-1}$ ), we estimate a  $0.02$  and  $0.03 \text{ ppb a}^{-1}$  annual mean decrease in surface  $\text{O}_3$  over NA and EA, respectively, or  $0.04$  and  $0.05 \text{ ppb a}^{-1}$  if EU CO and NMVOC emissions follow the EU  $\text{NO}_x$  trend. We conclude that the Asian  $\text{NO}_x$  emission changes estimated by Richter *et al.* [2005], if accompanied by increases in the other  $\text{O}_3$  precursors over Asia, are consistent with annual mean  $\text{O}_3$  trends of  $\sim 0.1 \text{ ppb a}^{-1}$ , but are insufficient to produce a  $0.5 \text{ ppb a}^{-1}$  trend. In a similar manner, we estimate that the 60% increase in south Asian  $\text{NO}_x$  emissions projected by the Current Legislation (CLE) emission scenario between 2005 and 2030 [Dentener *et al.*, 2005; Cofala *et al.*, 2005] to result from growth in the power and transportation sectors would increase surface  $\text{O}_3$  over NA, EU, and EA by less than  $0.3 \text{ ppb}$ .

[47] Trends derived from measurements at remote sites situated on the western coasts of North America and Europe, or on mountain summits where they sample free tropospheric air, are probably not representative of the spatial average over the large continental regions considered here. The intercontinental signal at such sites may be larger than in surface air over regions where  $\text{O}_3$  is subjected to higher depositional and chemical loss rates. In addition to rising anthropogenic emissions, regional changes in climate, biogenic emissions and wildfires may contribute to the observed  $\text{O}_3$  trends [e.g., Jaffe and Ray, 2007; Jaffe *et al.*, 2008]. Future studies should incorporate variability in both meteorology and emissions (including anthropogenic, biogenic, and wildfire) to explore whether models can attribute fully the observed increases in northern midlatitude surface  $\text{O}_3$  over the past decades, particularly given the growing demand for future projections of climate- and emission-driven changes in surface  $\text{O}_3$ .

## 8. Conclusions

[48] Under the umbrella of the Task Force on Hemispheric Transport of Air Pollution (TF HTAP; www.htap.org), we have used an ensemble modeling approach to estimate the impact of precursor emissions from four continental-scale

northern midlatitude source regions on surface O<sub>3</sub> levels in the same four receptor regions (Figure 1). Specifically, 21 global and hemispheric chemical transport models used meteorology for 2001 to simulate the impact of 20% decreases in “conventional” O<sub>3</sub> precursor emissions (NO<sub>x</sub>, NMVOC, and CO individually and combined) from east Asia (EA), Europe (EU), North America (NA) and south Asia (SA) on surface O<sub>3</sub> in the same four regions. Our results are intended to provide a first comprehensive assessment of annual and seasonal mean O<sub>3</sub> responses to changes in emissions from other continents, to gauge uncertainty in these estimates, and to serve as a benchmark for future work. The consistent approach applied in our study narrows the wide range of O<sub>3</sub> responses to changes in emissions on other continents reported in the literature (Figure 11). We identified a systematic model overestimate of surface O<sub>3</sub> concentrations compared to observations over the eastern United States and Japan (Figure 2), and show that the bias within individual models does not correlate with the strength of the O<sub>3</sub> response to reductions in foreign emissions. We find a strong sensitivity to uncertainties in anthropogenic NMVOC emissions, particularly over EU (Figure 10). The magnitude of simulated O<sub>3</sub> responses both to foreign and domestic emissions typically varies by at least a factor of two across the models (Figures 3 and 11). Reducing this uncertainty requires additional work to identify observational constraints that would distinguish which models best represent the key processes for hemispheric transport of O<sub>3</sub>.

[49] In addition to the precursors that are traditionally regulated to abate O<sub>3</sub> pollution (i.e., NO<sub>x</sub>, NMVOC, and CO), we examined the contribution of CH<sub>4</sub> to hemispheric-wide surface O<sub>3</sub> levels, both directly by changing global CH<sub>4</sub> abundances, and indirectly through the influence that the traditional O<sub>3</sub> precursors have on OH concentrations, and thereby the CH<sub>4</sub> abundance [e.g., Prather, 1996]. Owing to competing effects of CO and NMVOC versus NO<sub>x</sub> on OH, neglecting the long-term feedback when equivalent percentages of CO, NMVOC and NO<sub>x</sub> are reduced together introduces errors of at most a few percent. Given the different anthropogenic sources of NO<sub>x</sub>, CO, and NMVOC, application of equivalent percentage reductions to all three precursors may not be pragmatic, in which case the long-term effect may not be trivial. We further show that the responses to single-component versus multicomponent emission reductions are approximately equivalent for the O<sub>3</sub> responses to changes in domestic and foreign emissions (Figure 8), although the multicomponent response is less-than-linear in coupled aerosol simulations in which aerosols and their precursors were also decreased. We focus the remainder of our conclusions on the simulations with the combined reductions of NO<sub>x</sub>, CO, and NMVOC.

[50] We define a continental-scale “import sensitivity” as the ratio of the sum of the change in surface O<sub>3</sub> resulting from perturbations to precursor emissions in the three foreign source regions to the surface O<sub>3</sub> change resulting from the same perturbations to domestic emissions. Regional O<sub>3</sub> production reaches a maximum in summer over EA, EU, and NA (Figure 5; ensemble regional mean O<sub>3</sub> decreases of 1.3–1.8 ppb), with import sensitivities for July of 0.2 (NA and EA) to 0.3 (EU) (Figure 7). We assign a high degree of uncertainty, however, to the NA and EA results given the model bias compared to surface observations during the

summer and early fall (Figure 2). The model ensemble mean import sensitivity ranges from 0.5 (SA in November) to 1.1 (EA in March) during the month with the largest surface O<sub>3</sub> response to the combined foreign emission reductions (ensemble spatial mean decrease of 0.7–0.9 ppb versus 0.8–1.6 ppb O<sub>3</sub> decrease from the 20% reductions in domestic anthropogenic emissions during the same month).

[51] For all source regions, the model ensemble mean intercontinental influence is largest during spring and in late fall (Figure 6), consistent with prior studies (Figure 11 and section 1). The most robust rankings of intercontinental influence across the models are that surface O<sub>3</sub> levels over EU are influenced most strongly by emission reductions in NA, followed by EA, and that SA contributes least to the three foreign regions. We find more uncertainty in the relative importance of EA versus EU on NA, and of the three source regions over both Asian regions. Our analysis of the impact of decreases in anthropogenic emissions on the incidence of daily maximum 8-h average O<sub>3</sub> concentrations above 60 ppb (DAYS > 60) suggests that the annual and seasonal mean responses are qualitatively relevant for assessing air quality changes as measured by a threshold statistic used to gauge compliance with air quality standards. These high O<sub>3</sub> values, however, are much more sensitive to domestic emissions, even in spring (domestic emission reductions yield ~15–35% decreases from the base case whereas emission reductions in individual foreign source regions yield decreases of at most 5–10%).

[52] The annual mean responses to emission reductions of the traditional O<sub>3</sub> precursors from a single foreign source region are often 10% (maximum of ~50%) of the responses to domestic emission reductions (Figure 3). From the model ensemble annual mean response to a 20% decrease in global CH<sub>4</sub> abundances, we infer that the O<sub>3</sub> decrease over foreign regions produced by regional reductions in anthropogenic CH<sub>4</sub> emissions is roughly equivalent to the O<sub>3</sub> decrease from the same percentage reduction of NO<sub>x</sub>, NMVOC, and CO together. We emphasize that these results are large spatial averages that may not convey the larger foreign influence occurring in some subcontinental regions (e.g., the west coasts of NA and EU). Our results provide a baseline for future assessments of the surface O<sub>3</sub> response to emission changes on foreign continents, a key step toward determining the interaction of domestic efforts to improve air quality with emission changes occurring elsewhere in the globe.

[53] **Acknowledgments.** We are grateful to D. Jaffe and D. Reidmiller (University of Washington), and to A. Gnanadesikan and R. Stouffer (GFDL) and three anonymous reviewers for insightful comments on previous versions of the manuscript. C.A. and D.B. were supported primarily by the U.S. DOE Atmospheric Science Program (Office of Science, BER) at LLNL under contract DE-AC52-07NA27344. R.M.D., I.A.M., and D.S.S. acknowledge funding from NERC (NE/D012538/1); B.N.D. from NASA MAP; M.G.S., K.J.P., and W.J.C. from the UK Defra under contract AQ902 and the Joint DECC and MoD Programme, (DECC) GA01101 (MoD) CBC/2B/0417\_Annex C5; A.L. and J.W.K. from the Canadian Foundation for Climate and Atmospheric Sciences, the Ontario Ministry of the Environment, the Canadian Foundation for Innovation and the Ontario Innovation Trust; and M.G.V. from the Spanish Ministry of the Environment. R.J.P. was partly supported by the Korea Meteorological Administration Research and Development Program under grant CATER 2007–3205.

## References

Akimoto, H. (2003), Global air quality and pollution, *Science*, 302, 1716–1719, doi:10.1126/science.1092666.

- Auvray, M., and I. Bey (2005), Long-range transport to Europe: Seasonal variations and implications for the European ozone budget, *J. Geophys. Res.*, *110*, D11303, doi:10.1029/2004JD005503.
- Bergin, M. S., J. J. West, T. J. Keating, and A. G. Russell (2005), Regional atmospheric pollution and transboundary air quality management, *Annu. Rev. Environ. Resour.*, *30*, 1–37, doi:10.1146/annurev.energy.30.050504.144138.
- Berntsen, T. K., S. Karlsdottir, and D. A. Jaffe (1999), Influence of Asian emissions on the composition of air reaching the North Western United States, *Geophys. Res. Lett.*, *26*, 2171–2174, doi:10.1029/1999GL900477.
- Bey, I., D. J. Jacob, J. A. Logan, and R. M. Yantosca (2001), Asian chemical outflow to the Pacific in spring: Origins, pathways, and budgets, *J. Geophys. Res.*, *106*(D19), 23,097–23,113, doi:10.1029/2001JD000806.
- Bowman, K. P., and G. D. Carrie (2002), The mean-meridional transport circulation of the troposphere in an idealized GCM, *J. Atmos. Sci.*, *59*, 1502–1514, doi:10.1175/1520-0469(2002)059<1502:TMMTCO>2.CO;2.
- Carlsaw, D. C. (2005), On the changing seasonal cycles and trends of ozone at Mace Head Ireland, *Atmos. Chem. Phys.*, *5*, 3441–3450.
- Cofala, J., M. Amann, and Z. Klimont (2005), Scenarios of world anthropogenic emissions of SO<sub>2</sub>, NO<sub>x</sub>, and CO up to 2030, internal report, p. 17, Transboundary Air Pollut. Programme, Int. Inst. for Appl. Syst. Anal., Laxenburg, Austria. (Available at [http://www.iiasa.ac.at/rains/global\\_emiss/global\\_emiss.html](http://www.iiasa.ac.at/rains/global_emiss/global_emiss.html))
- Collins, W. J., D. S. Stevenson, C. E. Johnson, and R. G. Derwent (2000), The European regional ozone distribution and its links with the global scale for the years 1992 and 2015, *Atmos. Environ.*, *34*, 255–267, doi:10.1016/S1352-2310(99)00226-5.
- Collins, W. J., R. G. Derwent, C. E. Johnson, and D. S. Stevenson (2002), The oxidation of organic compounds in the troposphere and their global warming potentials, *Clim. Change*, *52*, 453–479, doi:10.1023/A:1014221225434.
- Cooper, O. R., and J. L. Moody (2000), Meteorological controls on ozone at an elevated eastern United States regional background monitoring site, *J. Geophys. Res.*, *105*(D5), 6855–6869, doi:10.1029/1999JD901015.
- Crutzen, P. (1973), A discussion of the chemistry of some minor constituents in the stratosphere and troposphere, *Pure Appl. Geophys.*, *106–108*, 1385–1399, doi:10.1007/BF00881092.
- Daniel, J. S., and S. Solomon (1998), On the climate forcing of carbon monoxide, *J. Geophys. Res.*, *103*(D11), 13,249–13,260, doi:10.1029/98JD00822.
- Denman, K. L., et al. (2007), Couplings between changes in the climate system and biogeochemistry, in *Climate Change 2007: The Physical Science Basis, Contribution of Working Group I to the Fourth Assessment Report of the Intergovernmental Panel on Climate Change*, edited by S. Solomon et al., pp. 499–587, Cambridge Univ. Press, Cambridge, U.K.
- Dentener, F., D. Stevenson, J. Cofala, R. Mechler, M. Amann, P. Bergamaschi, F. Raes, and R. Derwent (2005), The impact of air pollutant and methane emission controls on tropospheric ozone and radiative forcing: CTM calculations for the period 1990–2030, *Atmos. Chem. Phys.*, *5*, 1731–1755.
- Dentener, F., et al. (2006), The global atmospheric environment for the next generation, *Environ. Sci. Technol.*, *40*, 3586–3594, doi:10.1021/es0523845.
- Derwent, R. G., P. G. Simmonds, S. Seuring, and C. Dimmer (1998), Observation and interpretation of the seasonal cycles in the surface concentrations of ozone and carbon monoxide at Mace Head, Ireland from 1990 to 1994, *Atmos. Environ.*, *32*, 145–157, doi:10.1016/S1352-2310(97)00338-5.
- Derwent, R. G., W. J. Collins, C. E. Johnson, and D. S. Stevenson (2001), Transient behaviour of tropospheric ozone precursors in a global 3-D CTM and their indirect greenhouse effects, *Clim. Change*, *49*, 463–487, doi:10.1023/A:1010648913655.
- Derwent, R. G., et al. (2002), Coupling between the global and regional scale ozone distributions over Europe and the role of intercontinental transport, paper presented at Workshop on Hemispheric Pollution, U.S. Environ. Prot. Agency, Washington, D. C.
- Derwent, R. G., M. E. Jenkin, S. M. Saunders, M. J. Pilling, P. G. Simmonds, N. R. Passant, G. J. Dollard, P. Dumitrescu, and A. Kent (2003), Photochemical ozone formation in north west Europe and its control, *Atmos. Environ.*, *37*, 1983–1991, doi:10.1016/S1352-2310(03)00031-1.
- Derwent, R. G., et al. (2004), Intercontinental transport and the origins of the ozone observed at surface sites in Europe, *Atmos. Environ.*, *38*, 1891–1901, doi:10.1016/j.atmosenv.2004.01.008.
- Derwent, R. G., et al. (2006), External influences on Europe's air quality: Baseline methane, carbon monoxide and ozone from 1990 to 2030 at Mace Head, Ireland, *Atmos. Environ.*, *40*, 844–855, doi:10.1016/j.atmosenv.2005.09.077.
- Derwent, R. G., P. G. Simmonds, A. J. Manning, and T. G. Spain (2007), Trends over a 20-year period from 1987–2007 in surface ozone at the atmospheric research station, Mace Head, Ireland, *Atmos. Environ.*, *41*, 9091–9098, doi:10.1016/j.atmosenv.2007.08.008.
- Duncan, B. N., J. J. West, Y. Yoshida, A. M. Fiore, and J. R. Ziemke (2008), The influence of European pollution on ozone in the Near East and northern Africa, *Atmos. Chem. Phys.*, *8*, 2267–2283.
- Ellingsen, K., et al. (2008), Global ozone and air quality: A multi-model assessment of risks to human health and crops, *Atmos. Chem. Phys. Discuss.*, *8*, 2163–2223, [www.atmos-chem-phys-discuss.net/8/2163/2008/](http://www.atmos-chem-phys-discuss.net/8/2163/2008/).
- Fiore, A. M., D. J. Jacob, B. D. Field, D. G. Streets, S. D. Fernandes, and C. Jang (2002a), Linking air pollution and climate change: The case for controlling methane, *Geophys. Res. Lett.*, *29*(19), 1919, doi:10.1029/2002GL015601.
- Fiore, A. M., D. J. Jacob, I. Bey, R. M. Yantosca, B. D. Field, A. C. Fusco, and J. G. Wilkinson (2002b), Background ozone over the United States in summer: Origin, trend, and contribution to pollution episodes, *J. Geophys. Res.*, *107*(D15), 4275, doi:10.1029/2001JD000982.
- Fiore, A., D. J. Jacob, H. Liu, R. M. Yantosca, T. D. Fairlie, and Q. Li (2003), Variability in surface ozone background over the United States: Implications for air quality policy, *J. Geophys. Res.*, *108*(D24), 4787, doi:10.1029/2003JD003855.
- Fiore, A. M., J. J. West, L. W. Horowitz, V. Naik, and M. D. Schwarzkopf (2008), Characterizing the tropospheric ozone response to methane emission controls and the benefits to climate and air quality, *J. Geophys. Res.*, *113*, D08307, doi:10.1029/2007JD009162.
- Fuglestedt, J. S., et al. (1999), Climatic forcing of nitrogen oxides through changes in tropospheric ozone and methane: Global model studies, *Atmos. Environ.*, *33*, 961–967, doi:10.1016/S1352-2310(98)00217-9.
- Goldstein, A. H., et al. (2004), Impact of Asian emissions on observations at Trinidad Head, California, during ITCT 2K2, *J. Geophys. Res.*, *109*, D23S17, doi:10.1029/2003JD004406.
- Guerova, G., I. Bey, J.-L. Attié, R. V. Martin, J. Cui, and M. Sprenger (2006), Impact of transatlantic transport episodes on summertime ozone in Europe, 2057–2072, *Atmos. Chem. Phys.*, *6*, 2057–2072.
- Han, Z., et al. (2008), MICS-Asia II: Model intercomparison and evaluation of ozone and relevant species, *Atmos. Environ.*, *42*, 3491–3509, doi:10.1016/j.atmosenv.2007.07.031.
- Hess, P. (2005), A comparison of two paradigms: The relative global roles of moist convective versus nonconvective transport, *J. Geophys. Res.*, *110*, D20302, doi:10.1029/2004JD005456.
- Hess, P., and J.-F. Lamarque (2007), Ozone source attribution and its modulation by the Arctic Oscillation during the spring months, *J. Geophys. Res.*, *112*, D11303, doi:10.1029/2006JD007557.
- Holloway, T., A. Fiore, and M. Galanter Hastings (2003), Intercontinental transport of air pollution: Will emerging science lead to a new hemispheric treaty?, *Environ. Sci. Technol.*, *37*, 4535–4542, doi:10.1021/es034031g.
- Holloway, T., et al. (2008), MICS-Asia II: Impact of global emissions on regional air quality in Asia, *Atmos. Environ.*, *42*, 3543–3561, doi:10.1016/j.atmosenv.2007.10.022.
- Holzer, M., T. M. Hall, and R. B. Stull (2005), Seasonality and weather-driven variability of transpacific transport, *J. Geophys. Res.*, *110*, D23103, doi:10.1029/2005JD006261.
- Huntrieser, H., et al. (2005), Intercontinental air pollution transport from North America to Europe: Experimental evidence from airborne measurements and surface observations, *J. Geophys. Res.*, *110*, D01305, doi:10.1029/2004JD005045.
- Husar, R., et al. (2001), Asian dust events of April 1998, *J. Geophys. Res.*, *106*(D16), 18,317–18,330, doi:10.1029/2000JD900788.
- Jacob, D. J., L. W. Horowitz, J. W. Munger, B. G. Heikes, R. R. Dickerson, R. S. Artz, and W. C. Keene (1995), Seasonal transition from NO<sub>x</sub>- to hydrocarbon-limited conditions for ozone production over the eastern United States in September, *J. Geophys. Res.*, *100*(D5), 9315–9324, doi:10.1029/94JD03125.
- Jacob, D. J., J. A. Logan, and P. P. Murti (1999), Effect of rising Asian emissions on surface ozone in the United States, *Geophys. Res. Lett.*, *26*, 2175–2178, doi:10.1029/1999GL900450.
- Jaeglé, L., D. A. Jaffe, H. U. Price, P. Weiss-Penzias, P. I. Palmer, M. J. Evans, D. J. Jacob, and I. Bey (2003), Sources and budgets for CO and O<sub>3</sub> in the northeast Pacific during the spring of 2001: Results from the PHOBEA-II Experiment, *J. Geophys. Res.*, *108*(D20), 8802, doi:10.1029/2002JD003121.
- Jaffe, D., and J. Ray (2007), Increase in surface ozone at rural sites in the western US, *Atmos. Environ.*, *41*, 5452–5463, doi:10.1016/j.atmosenv.2007.02.034.
- Jaffe, D. A., et al. (1999), Transport of Asian air pollution to North America, *Geophys. Res. Lett.*, *26*, 711–714, doi:10.1029/1999GL900100.
- Jaffe, D., J. Snow, and O. Cooper (2003a), The April 2001 Asian dust events: Transport and substantial impact on surface particulate matter concentrations across the United States, *Eos Trans. AGU*, *84*, 501, 507.
- Jaffe, D., I. McKendry, T. Anderson, and H. Price (2003b), Six 'new' episodes of trans-Pacific transport of air pollutants, *Atmos. Environ.*, *37*, 391–404, doi:10.1016/S1352-2310(02)00862-2.

- Jaffe, D. A., et al. (2003c), Increasing background ozone during spring on the west coast of North America, *Geophys. Res. Lett.*, *30*(12), 1613, doi:10.1029/2003GL017024.
- Jaffe, D., I. Bertsch, L. Jaeglé, P. Novelli, J. S. Reid, H. Tanimoto, R. Vingarzan, and D. L. Westphal (2004), Long-range transport of Siberian biomass burning emissions and impact on surface ozone in western North America, *Geophys. Res. Lett.*, *31*, L16106, doi:10.1029/2004GL020093.
- Jaffe, D. A., W. Hafner, D. Chand, A. Westerling, and D. Spracklen (2008), Influence of fires on O<sub>3</sub> concentrations in the western U.S., *Environ. Sci. Technol.*, *42*, 5885–5891, doi:10.1021/es800084k.
- Jonson, J. E., D. Simpson, H. Fagerli, and S. Solberg (2005), Can we explain the trends in European ozone levels?, *Atmos. Chem. Phys.*, *6*, 51–66.
- Keating, T. J., J. J. West, and A. E. Farrell (2004), *Intercontinental Transport of Air Pollution*, edited by A. Stohl, pp. 295–320, Springer, Berlin.
- Kunhikrishnan, T., M. G. Lawrence, R. von Kuhlmann, M. O. Wenig, A. H. Asman, A. Richter, and J. P. Burrows (2006), Regional NO<sub>x</sub> emission strength for the Indian subcontinent and the impact of emissions from India and neighboring countries on regional O<sub>3</sub> chemistry, *J. Geophys. Res.*, *111*, D15301, doi:10.1029/2005JD006036.
- Lelieveld, J., et al. (2002a), Global air pollution crossroads over the Mediterranean, *Science*, *298*, 794–799, doi:10.1126/science.1075457.
- Lelieveld, J., W. Peters, F. J. Dentener, and M. C. Krol (2002b), Stability of tropospheric hydroxyl chemistry, *J. Geophys. Res.*, *107*(D23), 4715, doi:10.1029/2002JD002272.
- Li, Q. B., et al. (2001), A tropospheric ozone maximum over the Middle East, *Geophys. Res. Lett.*, *28*, 3235–3238, doi:10.1029/2001GL013134.
- Li, Q., et al. (2002), Transatlantic transport of pollution and its effects on surface ozone in Europe and North America, *J. Geophys. Res.*, *107*(D13), 4166, doi:10.1029/2001JD001422.
- Lin, J.-T., D. J. Wuebbles, and X.-Z. Liang (2008), Effects of intercontinental transport on surface ozone over the United States: Present and future assessment with a global model, *Geophys. Res. Lett.*, *35*, L02805, doi:10.1029/2007GL031415.
- Liu, H., D. J. Jacob, L. Y. Chan, S. J. Oltmans, I. Bey, R. M. Yantosca, J. M. Harris, B. N. Duncan, and R. V. Martin (2002), Sources of tropospheric ozone along the Asian Pacific Rim: An analysis of ozonesonde observations, *J. Geophys. Res.*, *107*(D21), 4573, doi:10.1029/2001JD002005.
- Liu, H., D. J. Jacob, I. Bey, R. M. Yantosca, B. N. Duncan, and G. W. Sachse (2003), Transport pathways for Asian pollution outflow over the Pacific: Interannual and seasonal variations, *J. Geophys. Res.*, *108*(D20), 4786, doi:10.1029/2002JD003102.
- Liu, J., D. L. Mauzerall, and L. W. Horowitz (2005), Analysis of seasonal and interannual variability in transpacific transport, *J. Geophys. Res.*, *110*, D04302, doi:10.1029/2004JD005207.
- Naik, V., D. Mauzerall, L. Horowitz, M. D. Schwarzkopf, V. Ramaswamy, and M. Oppenheimer (2005), Net radiative forcing due to changes in regional emissions of tropospheric ozone precursors, *J. Geophys. Res.*, *110*, D24306, doi:10.1029/2005JD005908.
- Olivier, J. G. J., et al. (2005), Recent trends in global greenhouse gas emissions: Regional trends and spatial distribution of key sources, in *Non-CO<sub>2</sub> Greenhouse Gases (NCGG-4)*, edited by A. van Amstel, pp. 325–330, Millpress, Rotterdam, Netherlands.
- Oltmans, S. J., et al. (2006), Long-term changes in tropospheric ozone, *Atmos. Environ.*, *40*, 3156–3173, doi:10.1016/j.atmosenv.2006.01.029.
- Ordóñez, C., H. Mathis, M. Furger, S. Henne, C. Huglin, J. Staehelin, and A. S. H. Prévôt (2005), Changes of daily surface ozone maxima in Switzerland in all seasons from 1992–2002 and a discussion of summer 2003, *Atmos. Chem. Phys.*, *5*, 1187–1203.
- Parrish, D. D., et al. (2004), Changes in the photochemical environment of the temperate North Pacific troposphere in response to increased Asian emissions, *J. Geophys. Res.*, *109*, D23S18, doi:10.1029/2004JD004978.
- Pochanart, P., H. Akimoto, Y. Kajii, V. M. Potemkin, and T. V. Khodzher (2003), Regional background ozone and carbon monoxide variations in remote Siberia/East Asia, *J. Geophys. Res.*, *108*(D1), 4028, doi:10.1029/2001JD001412.
- Prather, M. J. (1996), Time scales in atmospheric chemistry: Theory, GWPs for CH<sub>4</sub> and CO, and runaway growth, *Geophys. Res. Lett.*, *23*, 2597–2600, doi:10.1029/96GL02371.
- Prather, M., et al. (2001), *Climate Change 2001: The Scientific Basis*, edited by J. T. Houghton et al., pp. 239–287, Cambridge Univ. Press, Cambridge, U.K.
- Prinn, R. G., et al. (2005), Evidence for variability of atmospheric hydroxyl radicals over the past quarter century, *Geophys. Res. Lett.*, *32*, L07809, doi:10.1029/2004GL022228.
- Prospero, J. M. (1999), Long-term measurements of the transport of African mineral dust to the southeastern United States: Implications for regional air quality, *J. Geophys. Res.*, *104*(D13), 15,917–15,927, doi:10.1029/1999JD900072.
- Reichler, T., and J. Kim (2008), How well do coupled models simulate today's climate?, *Bull. Am. Meteorol. Soc.*, *89*, 303–311, doi:10.1175/BAMS-89-3-303.
- Richter, A., et al. (2005), Increase in tropospheric nitrogen dioxide over China observed from space, *Nature*, *437*(7055), 129–132, doi:10.1038/nature04092.
- Sanderson, M., et al. (2008), A multi-model study of the hemispheric transport and deposition of oxidized nitrogen, *Geophys. Res. Lett.*, *35*, L17815, doi:10.1029/2008GL035389.
- Schultz, M. G., et al. (2007), REanalysis of the Tropospheric (RETRO) chemical composition over the past 40 years, *Rep. Earth Syst. Sci.* *48/2007*, 122 pp., Max Planck Inst. for Meteorol., Hamburg, Germany.
- Schulz, M., et al. (2006), Radiative forcing by aerosols as derived from the AeroCom present-day and pre-industrial simulations, *Atmos. Chem. Phys.*, *6*, 5225–5246.
- Shindell, D., et al. (2008), A multi-model assessment of pollution transport to the Arctic, *Atmos. Chem. Phys.*, *8*, 5353–5372.
- Sillman, S. (1999), The relation between ozone, NO<sub>x</sub> and hydrocarbons in urban and polluted rural environments, *Atmos. Environ.*, *33*, 1821–1845, doi:10.1016/S1352-2310(98)00345-8.
- Solberg, S., R. G. Derwent, O. Hov, J. Langner, and A. Lindskog (2005), European abatement of surface ozone in a global perspective, *Ambio*, *34*(1), 47–53.
- Spivakovsky, C. M., et al. (2000), Three-dimensional climatological distribution of tropospheric OH: Update and evaluation, *J. Geophys. Res.*, *105*(D7), 8931–8980, doi:10.1029/1999JD901006.
- Stevenson, D. S., R. M. Doherty, M. G. Sanderson, W. J. Collins, C. E. Johnson, and R. G. Derwent (2004), Radiative forcing from aircraft NO<sub>x</sub> emissions: Mechanisms and seasonal dependence, *J. Geophys. Res.*, *109*, D17307, doi:10.1029/2004JD004759.
- Stevenson, D. S., et al. (2006), Multi-model ensemble simulations of present-day and near-future tropospheric ozone, *J. Geophys. Res.*, *111*, D08301, doi:10.1029/2005JD006338.
- Stohl, A., S. Eckhardt, C. Forster, P. James, and N. Spichtinger (2002), On the pathways and timescales of intercontinental air pollution transport, *J. Geophys. Res.*, *107*(D23), 4684, doi:10.1029/2001JD001396.
- Sudo, K., and H. Akimoto (2007), Global source attribution of tropospheric ozone: Long-range transport from various source regions, *J. Geophys. Res.*, *112*, D12302, doi:10.1029/2006JD007992.
- Szopa, S., et al. (2006), Future global tropospheric ozone changes and impact on European air quality, *Geophys. Res. Lett.*, *33*, L14805, doi:10.1029/2006GL025860.
- Task Force on Hemispheric Transport of Air Pollution (2007), Hemispheric transport of air pollution 2007 interim report, edited by T. J. Keating and A. Zuber, *Air Pollut. Stud.* *16*, U.N. Econ. Comm. for Europe, New York.
- Trickl, T., O. R. Cooper, H. Eisele, P. James, R. Mücke, and A. Stohl (2003), Intercontinental transport and its influence on the ozone concentrations over central Europe: Three case studies, *J. Geophys. Res.*, *108*(D12), 8530, doi:10.1029/2002JD002735.
- Vingarzan, R. (2004), A review of surface ozone background levels and trends, *Atmos. Environ.*, *38*, 3431–3442, doi:10.1016/j.atmosenv.2004.03.030.
- Wang, Y., and D. J. Jacob (1998), Anthropogenic forcing on tropospheric ozone and OH since preindustrial times, *J. Geophys. Res.*, *103*(D23), 31,123–31,135, doi:10.1029/1998JD100004.
- Wang, Y., D. J. Jacob, and J. A. Logan (1998), Global simulation of tropospheric O<sub>3</sub>-NO<sub>x</sub>-hydrocarbon chemistry: 3. Origin of tropospheric ozone and effects of nonmethane hydrocarbons, *J. Geophys. Res.*, *103*(D9), 10,757–10,768, doi:10.1029/98JD00156.
- Weiss-Penzias, P., D. A. Jaffe, L. Jaeglé, and Q. Liang (2004), Influence of long-range-transported pollution on the annual and diurnal cycles of carbon monoxide and ozone at Cheeka Peak Observatory, *J. Geophys. Res.*, *109*, D23S14, doi:10.1029/2004JD004505.
- Weiss-Penzias, P., D. A. Jaffe, P. Swartzendruber, J. B. Dennison, D. Chand, W. Hafner, and E. Prestbo (2006), Observations of Asian air pollution in the free troposphere at Mount Bachelor Observatory during the spring of 2004, *J. Geophys. Res.*, *111*, D10304, doi:10.1029/2005JD006522.
- West, J. J., A. M. Fiore, V. Naik, L. W. Horowitz, M. D. Schwarzkopf, and D. L. Mauzerall (2007), Ozone air quality and radiative forcing consequences of changes in ozone precursor emissions, *Geophys. Res. Lett.*, *34*, L06806, doi:10.1029/2006GL029173.
- Wild, O. (2007), Modelling the global tropospheric ozone budget: Exploring the variability in current models, *Atmos. Chem. Phys.*, *7*, 2643–2660.
- Wild, O., and H. Akimoto (2001), Intercontinental transport of ozone and its precursors in a three-dimensional globe CTM, *J. Geophys. Res.*, *106*(D21), 27,729–27,744, doi:10.1029/2000JD000123.
- Wild, O., and M. J. Prather (2000), Excitation of the primary tropospheric chemical mode in a global three-dimensional model, *J. Geophys. Res.*, *105*(D20), 24,647–24,660, doi:10.1029/2000JD900399.

- Wild, O., M. J. Prather, and H. Akimoto (2001), Indirect long-term global radiative cooling from NO<sub>x</sub> emissions, *Geophys. Res. Lett.*, 28, 1719–1722, doi:10.1029/2000GL012573.
- Wild, O., J. K. Sundet, M. J. Prather, I. S. A. Isaksen, H. Akimoto, E. V. Browell, and S. J. Oltmans (2003), Chemical transport model ozone simulations for spring 2001 over the western Pacific: Comparisons with TRACE-P lidar, ozonesondes, and TOMS columns, *J. Geophys. Res.*, 108(D21), 8826, doi:10.1029/2002JD003283.
- Wild, O., P. Pochanart, and H. Akimoto (2004), Trans-Eurasian transport of ozone and its precursors, *J. Geophys. Res.*, 109, D11302, doi:10.1029/2003JD004501.
- Wilkening, K. E., et al. (2000), Atmospheric science: Trans-Pacific air pollution, *Science*, 290, 65–67, doi:10.1126/science.290.5489.65.
- World Health Organization (2005), WHO air quality guidelines global update, report on a working group meeting, Bonn, Germany, 18–20 October, 2005, *Rep. E87950*, 25 pp., Geneva.
- Wu, S., L. J. Mickley, D. J. Jacob, J. A. Logan, R. M. Yantosca, and D. Rind (2007), Why are there large differences between models in global budgets of tropospheric ozone?, *J. Geophys. Res.*, 112, D05302, doi:10.1029/2006JD007801.
- Yienger, J., M. Galanter, T. Holloway, M. Phadnis, S. Guttikunda, G. Carmichael, W. Moxim, and H. Levy II (2000), The episodic nature of air pollution transport from Asia to North America, *J. Geophys. Res.*, 105(D22), 26,931–26,945, doi:10.1029/2000JD900309.
- C. Atherton, Gordon and Betty Moore Foundation, Presidio of San Francisco, P.O. Box 29910, San Francisco, CA 94129-0910, USA. (Cynthia.Atherton@moore.org)
- D. Bergmann, Atmospheric Earth and Energy Division, Lawrence Livermore National Laboratory, P.O. Box 808, Livermore, CA 94551-0808, USA. (dbergmann@llnl.gov)
- I. Bey, Laboratoire de Modélisation de la Chimie Atmosphérique, EPFL, Station 2, CH-1015 Lausanne, Switzerland. (isabelle.bey@epfl.ch)
- G. Carmichael, Center for Global and Regional Environmental Research, College of Engineering, University of Iowa, Iowa City, IA 52242, USA. (gcarmich@engineering.uiowa.edu)
- W. J. Collins, G. Folberth, and M. G. Sanderson, Met Office Hadley Centre, Fitzroy Road, Exeter EX1 3PB, UK. (bill.collins@metoffice.gov.uk; gerd.folberth@metoffice.gov.uk; Michael.sanderson@metoffice.gov.uk)
- C. Cuvelier, F. J. Dentener, E. Marmer and R. Van Dingenen, Institute for Environment and Sustainability, DG-Joint Research Centre, European Commission, I-21020 Ispra, Italy. (kees.cuvelier@jrc.it; frank.dentener@jrc.it; elina.marmer@jrc.it; rita.van-dingenen@jrc.it)
- R. M. Doherty, I. A. MacKenzie, and D. S. Stevenson, School of GeoSciences, University of Edinburgh, Edinburgh EH9 3JN, UK. (ruth.doherty@ed.ac.uk; iamack@staffmail.ed.ac.uk; dstevens@staffmail.ed.ac.uk)
- B. N. Duncan, UMBC Goddard Earth Sciences and Technology Center, Code 613.3, NASA Goddard Space Flight Center, Greenbelt, MD 20771, USA. (Bryan.N.Duncan@nasa.gov)
- G. Faluvegi and D. T. Shindell, NASA Goddard Institute for Space Studies, 2880 Broadway, New York, NY 10025, USA. (greg.faluvegi@gmail.com; dshindell@giss.nasa.gov)
- A. M. Fiore and L. W. Horowitz, NOAA Geophysical Fluid Dynamics Laboratory, 201 Forrestal Road, Princeton, NJ 08542-0308, USA. (Arlene.Fiore@noaa.gov; Larry.Horowitz@noaa.gov)
- M. Gauss and I. S. A. Isaksen, Department of Geosciences, University of Oslo, P.O. Box 1022 Blindern, N-0315 Oslo, Norway. (Michael.gauss@geo.uio.no; ivar.isaksen@geofysikk.uio.no)
- S. Gong, Air Quality Research Division, Science and Technology Branch, Environment Canada, 4905 Dufferin Street, Toronto, ON M3H 5T4, Canada. (Sunling.Gong@ec.gc.ca)
- D. Hauglustaine, Life, Earth and Environmental Sciences, European Science Foundation, 1 quai Lezay-Marnésia, BP 90015, F-67080 Strasbourg CEDEX, France. (dhauglustaine@esf.org)
- P. Hess, Biological and Environmental Engineering, Cornell University, 312 Riley Robb, Ithaca, NY 14853-5701, USA. (hess@ucar.edu)
- T. Holloway, Center for Sustainability and the Global Environment, Nelson Institute for Environmental Studies, University of Wisconsin-Madison, 1710 University Avenue, Room 201A, Madison, WI 53726, USA. (taholloway@wisc.edu)
- D. J. Jacob, Atmospheric Chemistry Modeling Group, Harvard University, 29 Oxford Street, Cambridge, MA 02138, USA. (djacob@fas.harvard.edu)
- J. E. Jonson and P. Wind, Norwegian Meteorological Institute, P.O. Box 43 Blindern, N-0313 Oslo, Norway. (jan.eiof.jonson@met.no; peter.wind@met.no)
- J. W. Kaminski and A. Lupu, Center for Research in Earth and Space Science, York University, 4700 Keele Street, Toronto, ON M3J 1P3, Canada. (jacek@yorku.ca; alexlupu@yorku.ca)
- T. J. Keating, Office of Air and Radiation, Environmental Protection Agency, 1200 Pennsylvania Avenue, NW, Mail Code 6103A, Room 5442, Washington, DC 20460, USA. (Keating.Terry@epamail.epa.gov)
- V. Montanaro and G. Pitari, Department of Physics, University of L'Aquila, via Vetoio, I-67010 Coppito-L'Aquila, Italy. (veronica.montanaro@aquila.infn.it; gianni.pitari@aquila.infn.it)
- R. J. Park, School of Earth and Environmental Sciences, Seoul National University, San 56-1, Sillim, Gwanakgu, Seoul 151-742, South Korea. (rjpark@snu.ac.kr)
- K. J. Pringle, Max-Planck-Institut für Chemie, Joh.-J.-Becher-Weg 27, Universitätscampus, D-55128 Mainz, Germany. (pringle@mpch-mainz.mpg.de)
- J. A. Pyle, National Centre for Atmospheric Science, Department of Chemistry, University of Cambridge, Lensfield Road, Cambridge CB2 1EW, UK. (John.Pyle@atm.ch.cam.ac.uk)
- S. Schroeder and M. G. Schultz, ICG-II, Forschungszentrum Jülich, Leo Brandt Strasse, D-52425 Jülich, Germany. (s.schroeder@fz-juelich.de; m.schultz@fz-juelich.de)
- M. Schulz and S. Szopa, Laboratoire des Sciences du Climat et de l'Environnement, CEA, IPSL, UVSQ, CNRS, L'Orme des Merisiers, Bat 712, Point courrier 132, F-91191 Gif-sur-Yvette, France. (michael.schulz@isce.ipsl.fr; sophie.szopa@lsce.ipsl.fr)
- C. Textor, GMES France Atmosphère, Service d'Aéronomie, INSU, Tour 46, RDC 2, Université Pierre et Marie Curie, CNRS, Boite 102, 4 Place Jussieu, F-75252 Paris CEDEX 05, France. (christiane.textor@aero.jussieu.fr)
- M. G. Vivanco, Atmospheric Pollution Unit, CIEMAT, Avenida Complutense 22, E-28040 Madrid, Spain. (m.garcia@ciemat.es)
- O. Wild, Department of Environmental Science, Lancaster University, Lancaster Environment Centre, Lancaster LA1 4YQ, UK. (O.Wild@lancaster.ac.uk)
- G. Wojcik, Atmospheric Effects Group, Information Technology Sector, Northrop Grumman Corporation, 4801 Stonecroft Boulevard, Chantilly, VA 20151, USA. (gary.wojcik@ngc.com)
- S. Wu, Department of Geological and Mining Engineering and Sciences, Michigan Technological University, 1400 Townsend Drive, Houghton, MI 49931, USA. (slwu@mtu.edu)
- G. Zeng, National Institute of Water and Atmospheric Research Ltd., Private Bag 50061, Omakau, Central Otago, New Zealand.
- A. Zuber, Environment Directorate General, European Commission, Avenue de Beaulieu 5, B-1049 Brussels, Belgium. (Andre.ZUBER@ec.europa.eu)